DEPARTMENT OF MECHANICAL & AEROSPACE ENGINEERING

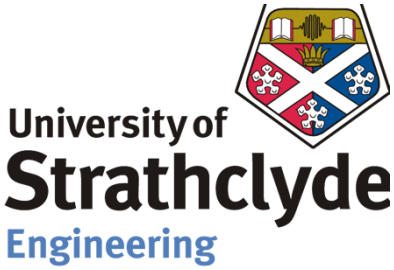

Department of Mechanical and Aerospace Engineering

Hydrogen Production from Seawater Electrolysis: Investigation of Potential Processes and Technologies

Author: Katie Berry

Supervisors: Dr Edward Brightman and Dr Paul Tuohy

A thesis submitted in partial fulfilment for the requirement of degree in

Master of Science in Sustainable Engineering: Renewable Energy Systems and the Environment

2021

Copyright Declaration

Signed: 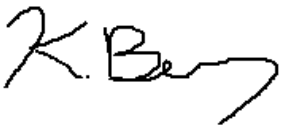 Date: 17/08/2021

Abstract

To reach the climate targets that have been set out by governments worldwide and keep global warming below 1.5^{o}C compared to pre-industrial levels, a greater level of renewable energy integration must be achieved. As an energy vector, hydrogen has the potential to help balance out renewable energy supply and decarbonise some areas such as heavy-duty transportation which are notoriously difficult to decarbonise. This report aims to investigate how the impending increase in hydrogen demand can be met sustainably by electrolysing seawater using either traditional technologies such as alkaline or PEM electrolysis or by using newer, membrane-less technologies. These membrane-less devices present benefits such as simplistic design and reduced component costs. A review of the literature found potential processes for producing hydrogen from seawater using traditional water purification methods, i.e. membrane filtration or thermal distillation, combined with alkaline or PEM electrolysers. Multiple membrane-less electrolyser devices intended for use in water electrolysis were also identified. Analysis of four separate processes for producing hydrogen from seawater found significant differences in terms of seawater throughput and energy efficiency between the processes. An alkaline electrolysis process yielded some of the best results with a water throughput of around 700 kg of seawater per kg of H2 and an overall energy efficiency of 34.8%. A process in which seawater vapour was electrolysed was deemed the least feasible due to the high water throughput and lack of economic benefits. A membrane-less electrolyser was incorporated into a process and it was found that although the electrolyser itself had a better energy efficiency than traditional electrolysers, the overall energy efficiency of the system was only approximately 2%. Despite this, the many attractive economic benefits of these electrolysers should not be overlooked. Finally, the relationship between flow regime, electrode separation distance and cell efficiency in membrane-less devices was explored, but it was found that no definitive conclusion could be made due to the small pool of data that was available.

Acknowledgements

I would firstly like to thank my supervisors, Dr Edward Brightman and Dr Paul Tuohy, who have supported me and guided me through this thesis. Dr Brightman initially recommended the topic of seawater electrolysis for hydrogen production to me and has helped throughout by sharing his expert knowledge with me and answering any queries I had on the subject. Dr Tuohy's support has also been invaluable not only during this project but throughout the entire Master's course. The materials taught by all lecturers in this course over the past two semesters were critical in producing this thesis project.

Additionally, I would like to thank Carl Fischer CEO of sHYp, who has kindly taken the time to provide useful resources regarding direct electrolysis of seawater and membrane-less electrolyser technologies and shared information regarding sHYp's own technology. His willingness to help has allowed me to produce a higher quality of work.

Table of Contents

List of Figures

List of Tables

Nomenclature

Abbreviation	Definition
Ar	Argon
BO_3^{3-}	Borate
Br^-	Bromide ion
C	Carbon
$Ca(OH)_2$	Calcium hydroxide
Ca^{2+}	Calcium ion
CAPEX	Capital expenditure
CCS	Carbon capture and storage
Cl^-	Chloride ion
Cl_2	Chlorine
ClER	Chlorine evolution reaction
ClO^-	Hypochlorite ion
Co	Cobalt
CO_2	Chlorine evolution reaction
CP	Centrifugal pump
CSP	Concentrating solar power
Cu	Copper
DEFT	Divergent electrode-flow-through
e^-	Electron
EES	Engineering Equation Solver
Fe	Iron
GA	Genetic algorithm
H^+	Hydron
H_2	Hydrogen
H_2O	Water
H_2SO_4	Sulfuric acid
HCO^{3-}	Bicarbonate ion

HDH	Humidification dehumidification
HER	Hydrogen evolution reaction
HHV	Higher heating value
HX	Heat exchanger
IEA	International Energy Agency
IPCC	Intergovernmental Panel on Climate Change
Ir	Iridium
IrO_2	Iridium dioxide
K^+	Potassium ion
KOH	Potassium hydroxide
LDH	Layered double hydroxide
LHV	Lower heating value
M	Molarity
MEA	Membrane electrode assembly
MFD	Multi-flash distillation
$Mg(OH)_2$	Magnesium hydroxide
Mg^{2+}	Magnesium ion
Mg_2SiO_4	Forsterite
Mn	Manganese
MW	Megawatt
N/A	Not applicable
N_2	Nitrogen
Na^+	Sodium ion
NaCl	Sodium chloride
NaOH	Sodium hydroxide
NF	Nanofiltration
Ni	Nickel
Ni200	Nickel alloy
O&M	Operation and maintenance
O_2	Oxygen

OER	Oxygen evolution reaction
OH^-	Hydroxide ion
ORC	Organic Rankine cycle
PCM	Phase change material
Pd	Palladium
PEM	Proton-exchange membrane
ppm	Parts per million
PSA	Pressure swing adsorption
Pt	Platinum
PTSC	Parabolic trough solar collector
PV	Photovoltaic
Rh	Rhodium
RH	Relative humidity
RO	Reverse osmosis
Ru	Ruthenium
RuO_2	Ruthenium dioxide
SiO_2	Silicon dioxide
SO_4^{2-}	Sulfate ion
Sr2+	Strontium ion
SW	Seawater
TDS	Total dissolved solids
TEG	Thermo-electric generator
Ti	Titanium
W	Tungsten
ZrO_2	Zirconium dioxide

List of Symbols

Symbol	Meaning	Units
A	Heat transfer area	m^2
C_P	Specific heat capacity at constant pressure	kJ/kg.K
C_V	Specific heat capacity at constant volume	kJ/kg.K
d	Diameter	m
J	Current density	mA/cm^2
K_{SP}	Solubility product	-
m	Mass	kg
m’	Mass flowrate	kg/s
MW	Molecular weight	g/mol
n’	Molar flowrate	mol/s
P	Pressure	Pa or bar
P_e	Electrical power	W
Q	Energy	kW or kJ/s
R	Resistance	Ω
Re	Reynolds’ number	-
T	Temperature	^oC or K
Tref	Reference temperature	K
u	Flow velocity	m/s
U	Overall heat transfer coefficient	$W/m^2.K$
V	Voltage or Volume	V or m^3
V’	Volumetric flowrate	m^3/s
γ	Specific heat ratio	-
ΔG^o_f	Standard Gibbs’ free energy of formation	kJ/mol
Δh_R	Reaction enthalpy change	kJ/mol
ΔT_{LM}	Log mean temperature difference	-
ε	Reaction conversion	-
η_C	Compressor efficiency	-
η_{CP}	Pump efficiency	-

μ	Dynamic viscosity	kg/m.s
ρ	Density	kg/m^3

1.0 Introduction

In December 2015, a legally binding international treaty known as the Paris Agreement was signed by 196 nations which agreed that global warming should be limited to well below 2°C in comparison to pre-industrial levels [1]. The Intergovernmental Panel on Climate Change (IPCC) have stated in their latest report that this limit is likely to be exceeded within the next few decades if emissions continue to climb [2]. Despite this, the current pledges made by the Paris Agreement do not align with the targets set by the IPCC and the International Energy Agency (IEA) have said that "we are far from on track" to achieving the goals set out [3]. It is therefore necessary to attain a higher degree of integration of renewable energy technologies.

As the most abundant element in the universe [4], hydrogen has the potential to overcome many of the obstacles currently faced in achieving net zero. It is an energy vector and therefore has endless applications, including as an energy storage solution [5]. Some of the many ways of producing, storing and utilising hydrogen are given in Figure 1.

Although the concept of a 'hydrogen economy' has been debated for decades, most hydrogen produced today is consumed as a chemical intermediate, dominantly in oil refining and ammonia production processes. As the global energy system transitions, hydrogen is likely to become much more in demand for sectors such as heating and heavy-duty transportation, due to its high energy density in comparison to fossil fuels; per kilogram, hydrogen contains around 2.6 times more energy than gasoline [6].

Once hydrogen is integrated into these industries and demand substantially increases, there will become an issue of producing hydrogen sustainably. There are four main pathways to producing hydrogen: brown, grey, blue and green. 'Brown' hydrogen involves coal gasification and is considered the least environmentally friendly and therefore least desirable of the pathways. Steam reforming of natural gas leads to the formation of 'grey' hydrogen, which becomes 'blue' hydrogen when the process is paired with carbon capture and storage (CCS). 'Green' hydrogen is produced when electrolysers use electricity from a renewable source to split water and is widely considered as the most favourable route to meeting the world's impending hydrogen demand; despite this, only 4% of hydrogen produced globally is currently derived from water electrolysis [7].

The electrolysis process was first discovered in the 19th century and today its most common applications are electrometallurgy (producing metals such as aluminium from their oxides) and

the chlor-alkali process (production of chlorine and sodium hydroxide). Alkaline electrolysers were the first technology to be used industrially and are still the most prevalent technology at a commercial level today [8]. Polymer electrolyte membrane (PEM) electrolyser cells were introduced in the 1960s as an alternative to alkaline electrolysers and present benefits such as high current densities and the ability to be fed by pure water rather than a caustic solution [9].

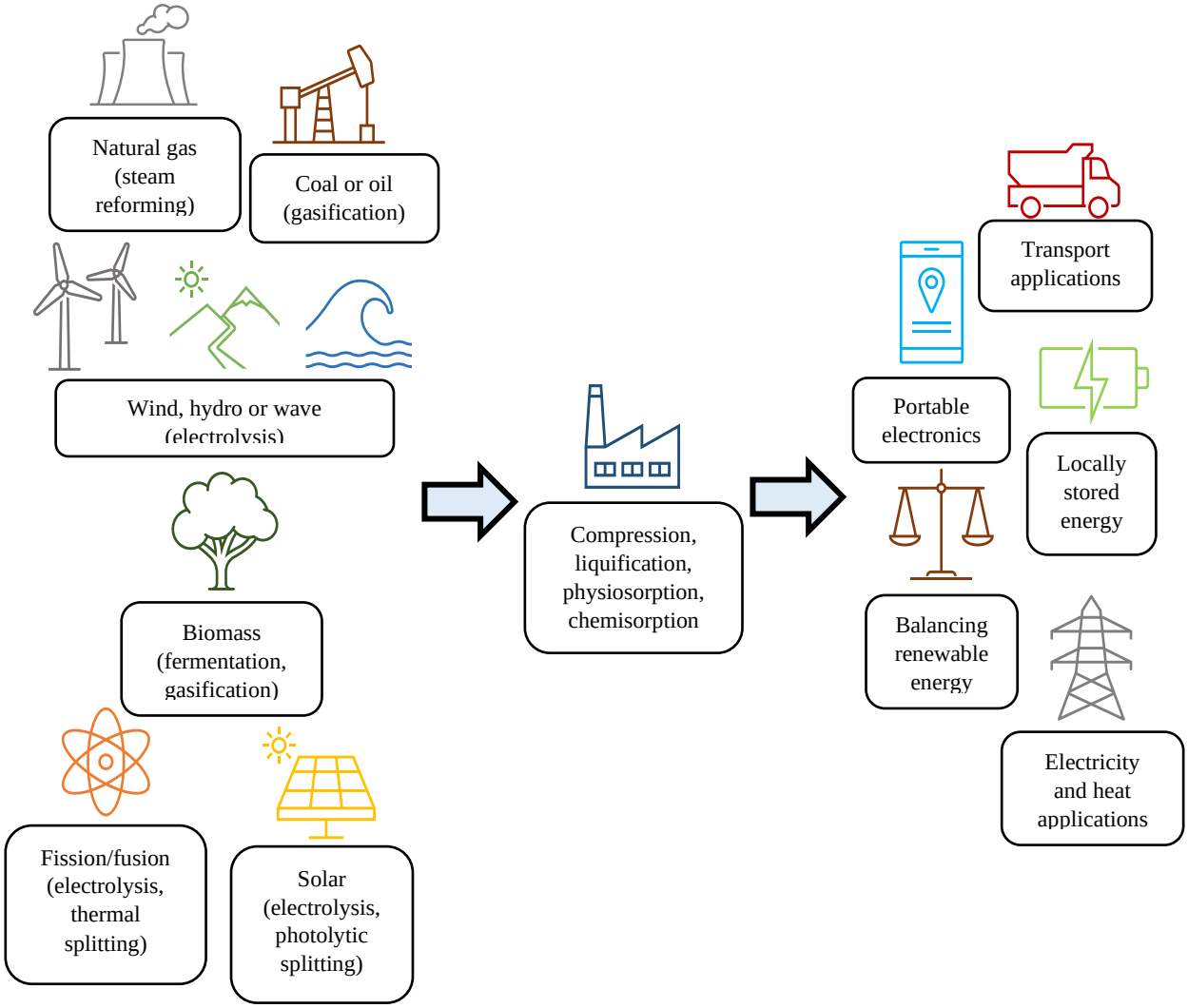

Figure 1 - Schematic showing possible methods of hydrogen production, storage and utilisation, created using information from [5].

Unfortunately, there are many drawbacks associated with producing hydrogen using these technologies. The use of a diaphragm or membrane leads to high component costs and low durability. Furthermore, PEM electrolysers can only operate with ultra-pure water that has a total dissolved solids (TDS) concentration of below 0.5 ppm or else the electrolyser membrane pores risk becoming clogged [10]. In many dry arid countries, freshwater is a scarce resource and they cannot afford to use this water to produce hydrogen.

It would therefore be beneficial if it was possible to produce hydrogen from seawater. This can be achieved by first purifying and filtering seawater before electrolytic splitting in a standard electrolyser. Alternatively, if an electrolyser was developed so that it could be used directly with seawater, it would remove this costly and energy intensive stage of distilling the water. Using an electrolyser without a membrane would not only reduce the costs and complexity of manufacturing, but it would also remove the issue of membrane pores becoming clogged and deactivating when electrolysing seawater, which is high in contaminants.

1.1 Issues Faced in Seawater Electrolysis

One of the main problems with using seawater as an electrolyte is that the high concentration of chloride (Cl^-) ions creates competition of the chlorine evolution reaction (ClER) with the preferred oxygen evolution reaction (OER) on the anode of the electrolysis cell [11] [12]. Although chlorine gas has many uses in industry, mass producing hydrogen via seawater electrolysis will likely create a supply of chlorine which outstrips demand [13]. While ClER can occur in acidic environments when electrolysing seawater, there is also the danger of hypochlorite (ClO^-) formation when performing electrolysis in an alkaline environment. Each of these reactions, presented in Equations 1 and 2 respectively, involve only two electrons per mole of product, whereas OER, shown in Equations 3 and 4, requires four electrons per mole of oxygen formed. This creates more favourable kinetics for ClER and hypochlorite formation in comparison to OER.

$$2Cl^- \rightarrow Cl_2 + 2e^- \quad (1)$$

$$Cl^- + 2OH^- \rightarrow ClO^- + H_2O + 2e^- \quad (2)$$

$$2H_2O \rightarrow O_2 + 4H^+ + 4e^- \ (acidic\ conditions) \quad (3)$$

$$4OH^- \rightarrow O_2 + 2H_2O + 4e^- (alkaline\ conditions) \quad (4)$$

Currently, the methods for inhibiting chlorine formation during the electrolysis of saline solutions or brine include operation at low current densities (< 1 mA/cm^2) [14], using electrocatalyst materials that prevent ClER [15] or using a cation exchange membrane layer on the anode to prevent Cl^- adsorption [16]. Operation at lower electrode potentials (and therefore lower current densities) inhibits ClER and promotes OER based on the Pourbaix diagram shown in Figure 1. However, this technique results in lower efficiencies and is therefore an inadequate solution as the process becomes economically unfeasible [13].

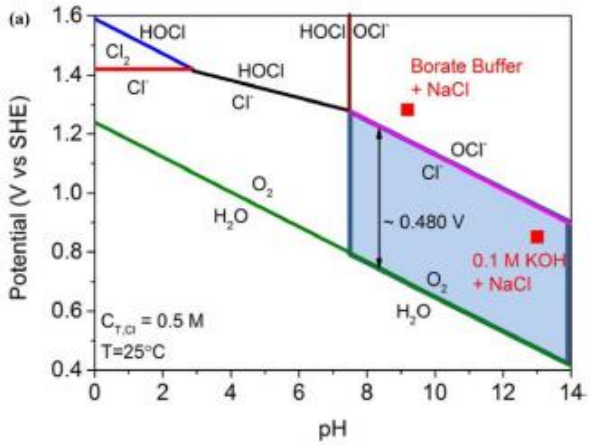

Figure 2 - Pourbaix diagram showing onset potentials for formation of oxygen, chlorine and hypochlorite in simulated seawater [17].

Furthermore, the high concentration of Cl^- creates aggressive conditions in which corrosion is highly likely, meaning robust electrocatalysts with high durability are necessary [18] [19]. In addition to this, the presence of other dissolved ions in seawater can lead to precipitation of alkaline earth metal hydroxides such as magnesium hydroxide ($Mg(OH_2)$) and calcium hydroxide ($Ca(OH)_2$), which can form on cathodes, blocking active sites for reactions and thereby reducing electrochemical activity [19] [20].

1.2 Types of Electrolysers

The two main types of electrolysers currently used in industry are alkaline electrolysers and proton-exchange membrane (PEM) electrolysers. The features and operating conditions of these two types of electrolysis are given in Table 1.

Table 1 - Operating conditions and other features of alkaline and PEM electrolysers.

Type of Electrolyser	Alkaline	PEM	Reference
Feed	20-40 wt% KOH solution	Pure water	[21]
Electrocatalyst	Ni, Cu, Mn, W, Ru	Pt, Ir, Ru, Rh	[21]
Separator	ZrO_2 with polysulphone polymer (Zirfon®)	Sulfonated tetrafluoroethylene based polymer (Nafion®)	[22] [23]
Cell temperature (°C)	30-80	20-80	[24]
Cell pressure (bara)	< 30	< 70	[24]

Max realised size (MW)	10	3	[25] [26] [27]
Efficiency (based on LHV)	70%	80%	[28]
Efficiency (kWh/kgH_2)	50-78	50-83	[24]
Current density (mA/cm^2)	250-450	1000-2000	[28]
Lifetime (1000 h)	60	50-80	[24]
CAPEX for stack (£/kW_{el})	196	290	[24]

The differences between these two types of electrolysis along with the advantages and disadvantages of each are explained in Sections 1.2.1 and 1.2.2.

1.2.1 Alkaline Electrolysis

Alkaline electrolysers are a mature technology and have been used commercially for almost a century. Potassium hydroxide solution (20-40 wt%) is pumped through the system as an electrolyte and facilitates the reactions which produce oxygen and hydrogen gas. Oxygen is produced as the anode when hydroxide (OH^-) ions are oxidised to become oxygen molecules, and hydrogen gas is the product of a reaction at the cathode in which water molecules are reduced to hydrogen molecules and hydroxide ions (Equations 5 to 7). The electrolyte and product gas mixture leave the cell and are separated in a gas separator. The gas is then purified via a demister or dryer, after which product purity can be over 99.5% [29] [30]. A schematic of this set up is given in Figure 2.

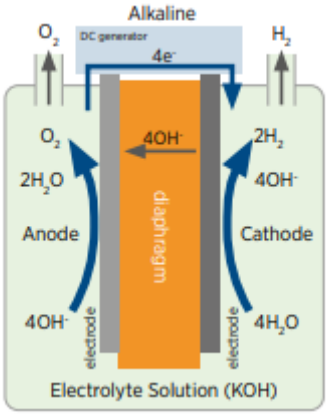

Figure 3 - Schematic showing operation of a typical alkaline electrolyser, taken from [24].

Previously, the two electrodes of an alkaline electrolysis cell were separated from the diaphragm by a defined distance, but modern versions of the technology are based on a zero-gap assembly in which the cathode and anode are attached to either side of the diaphragm. This

updated concept was designed to reduce Ohmic losses. The cell temperature can be anywhere between 30°C and 80°C and the maximum possible cell pressure is around 30 bar(a). The largest commercial single-stack alkaline electrolyser currently in operation is at the Fukushima Energy Research Field in Japan and is a 10 MW device. This stack is capable of producing green hydrogen gas at a rate of 1,200 Nm^3 per hour [31].

Anode:

$$2OH^-(aq) \rightarrow \frac{1}{2}O_2(g) + H_2O(l) + 2e^- \quad (5)$$

Cathode:

$$2H_2O(l) + 2e^- \rightarrow H_2(g) + 2OH^-(aq) \quad (6)$$

Overall reaction:

$$H_2O(l) \rightarrow H_2(g) + \frac{1}{2}O_2(g) \quad (7)$$

A full review of the state-of-the-art of alkaline electrolysis by Brauns and Turek can be found in [29].

1.2.2 Proton-Exchange Membrane (PEM) Electrolysis

The first solid polymer electrolyser was developed in the 1960s by General Electric and was intended to alleviate some of the issues faced by using alkaline electrolysers. A proton-conducting membrane, anode and cathode are combined in a cell to form a membrane-electrode assembly (MEA). The polymer electrolyte membrane is commonly made of Nafion®, which presents benefits such as high proton conductivity, allowing for a very thin membrane (~20-300 μm) to be used. Protons (H^+) are formed at the anode of the MEA and then transferred through the membrane to the cathode, where they recombine with the electrons to form hydrogen gas (Equations 8 to 10). No electrolyte is required in a PEM electrolyser as the membrane acts as an electrolyte, meaning pure water can be used for electrolysis.

Due to the corrosive, acidic environment induced by the proton exchange membrane, noble metal catalysts such as iridium and platinum must be used for the electrodes, thereby increasing the capital cost of the electrolyser stack. The biggest PEM electrolyser stack currently available is 3 MW but is likely to increase in the near future [32].

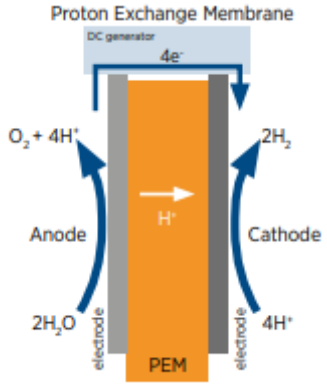

Figure 4 - Schematic showing the operation of a typical PEM electrolysis cell, taken from [24].

Anode:

$$H_2O(l) \rightarrow 2H^+(aq) + \frac{1}{2}O_2(g) + 2e^- \quad (8)$$

Cathode:

$$2H^+(aq) + 2e^- \rightarrow H_2(g) \quad (9)$$

Overall reaction:

$$H_2O(l) \rightarrow H_2(g) + \frac{1}{2}O_2(g) \quad (10)$$

Table 2 - Advantages and disadvantages of each type of electrolyser cell.

	Advantages	Disadvantages
Alkaline	• Mature technology • Low-cost technology (non-noble electrocatalysts, cheap electrolyte) • Long-term stability	• Low current densities • Formation of carbonates on electrode decreases performance • Cross-over of gases leads to lower product purity than other cell designs
PEM	• High current densities • Compact system design • Quick response time • Higher hydrogen production rate • Quick response time • Dynamic operation • High gas purity	• Expensive materials required for components (noble metal electrocatalysts) • High purity (< 0.5 ppm contaminants) water necessary • Acidic environment • Low durability

Reviews of the current state-of-the-art of PEM electrolysers used for hydrogen production have been carried out by Carmo et al [9] and Kumar and Himabindu [23]. A summary of the advantages and disadvantages of both types of electrolysers is given in Table 2.

1.3 Aims and Objectives

This thesis aims to explore two issues: hydrogen production from seawater and hydrogen production using membrane-less electrolyser devices. Various processes and technologies will be analysed based on factors such as energy efficiency and overall feasibility. The objectives are as follows:

- Identify four processes which show promise for producing hydrogen from seawater.
- Find the approximate energy and water consumption of these processes.
- Compare and contrast the processes based on efficiency and general feasibility.
- Gather information on all membrane-less technologies currently in commercial or research phase and compare the devices based on performance factors such as efficiency and flow regime.

Although economic factors will be touched upon in the analysis, a full economic review of the processes in question was considered out of scope of this project. This is because the cost of producing hydrogen via electrolysis is highly dependent on electricity prices which tend to fluctuate a lot depending on the area in which the electrolyser is based or the time of day or year, making it very difficult to predict.

2.0 Literature Review

A review of the available literature was conducted to identify any processes or technologies that are either in the research stage or commercially available for producing hydrogen from seawater. The review was divided into processes using membraned devices, membrane-less technologies for hydrogen production and electrocatalysts that are suitable for use with seawater. A software review was also carried out to investigate any potentially suitable software programs for carrying out the analysis.

2.1 Seawater Electrolysis Using Membraned Devices

One of the pathways proposed for electrolysis of seawater is combining standard industrial electrolysis technologies, such as alkaline or PEM electrolysers, with a filtration and

purification process to remove any potential harmful components. PEM electrolysers in particular have a very low tolerance to contaminants; they require a total dissolved solids (TDS) concentration of less than 0.5 ppm [10]. For reference, typical seawater has a TDS concentration of around 35,000 ppm [33]. Reverse osmosis, an electrically powered filtration process, produces water with a TDS concentration of around 400 to 600 ppm and is therefore not compatible with PEM [34]. However, desalination processes such as humidification and dehumidification or multi-effect distillation may be feasible options.

2.1.1 Alkaline Electrolysis Systems

Alkaline electrolysers have a higher tolerance to impurities and therefore do not require as complex purifications as PEM electrolysers. Additionally, using alkaline electrolysis systems for splitting seawater may be more convenient because the ions present in seawater can be used to form the alkaline electrolyte required for the process.

Amikam et al have developed a system for seawater electrolysis in which the operating conditions inhibit chlorine production and promote the more favourable oxygen production [13]. A schematic for the proposed process is given in Figure 5. Nanofiltration is used to completely remove Ca^{2+}, Mg^{2+} and SO_4^{2-} ions, as well as removing smaller fractions of K^+, Na^+ and Cl^- ions which are present in seawater. The filtered seawater is then passed into a settling tank containing sodium hydroxide solution at a concentration of 20 to 40 wt%, in which solid sodium chloride precipitates as a result of the common ion effect. From here, the sodium hydroxide solution enters the alkaline electrolyser, where oxygen and hydrogen are produced. The aqueous sodium hydroxide is then recycled back to the settling tank.

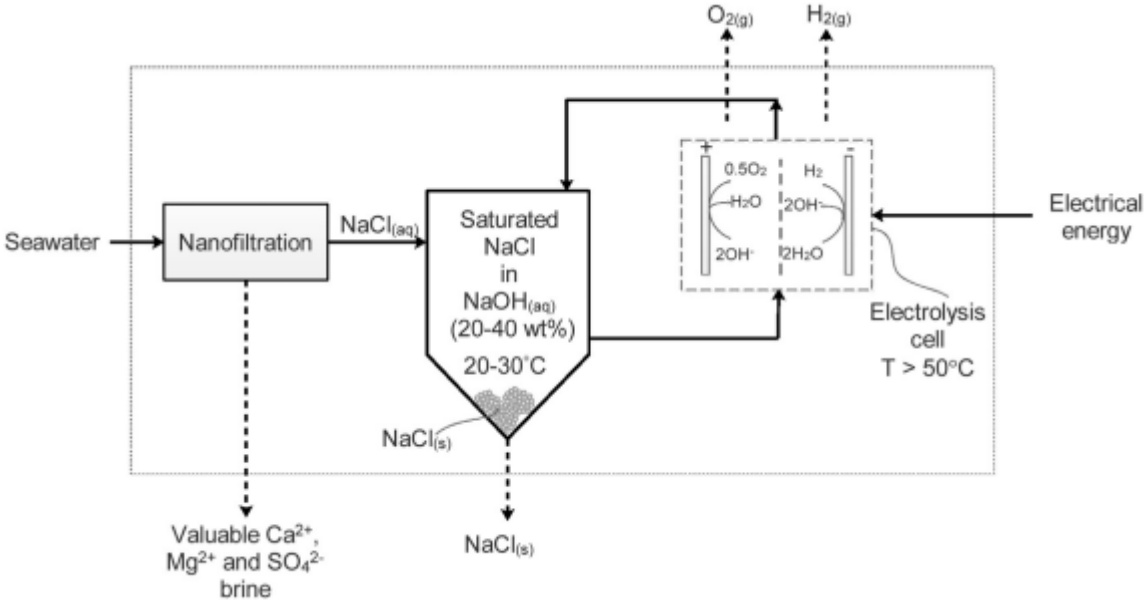

Figure 5 - Process diagram of chlorine-free alkaline electrolysis process [13].

The high concentration of hydroxide (OH^-) ions present in this system (< 2.5 M) prevents chlorine evolution on the anode. The electrolyser cell is operated at a higher temperature than the settling tank because sodium chloride's solubility increases with increasing temperature, so this prevents formation of solid sodium chloride in the electrolyser. A lab-scale experiment was set up to test this system and the results showed that at a concentration of 100 $gNaOH/kgH_2O$, no chlorine formed on the Ni200 and Ti/IrO_2-RuO_2-TiO_2 anodes after 12 days of operation. Furthermore, there was no accumulation of sodium chloride salt observed outside of the settling tank. However, during the experiment, the system was only tested using aqueous NaCl solution and not real seawater so, the effect of the accumulation of other ions present in seawater such as K^+ and Br^- is unknown. This design therefore requires further investigation before it can become feasible at a large scale.

2.1.2 PEM Electrolysis Systems

A hybrid solar thermal system that produces electricity and hydrogen from seawater has been proposed by Demir and Dincer [35]. Although the process was mainly designed with the objective of providing electricity, it is possible that it could be configured in a way so that hydrogen production is prioritised. The process is comprised of a concentrating solar power (CSP) gas turbine subsystem, multi-stage flash distillation (MFD), a PEM electrolyser and a thermoelectric generator (TEG) unit. The system operates as follows: air is compressed before being heated using CSP and is then passed through a gas turbine to generate electricity, which powers the electrolyser. The latent heat contained in the exhaust gas leaving the turbine is stored in a thermal storage system consisting of two phase change material (PCM) units. Seawater is pumped into the MFD unit where it is heated using the thermal energy stored in the PCM. The distilled water from this section is then passed into the PEM electrolyser where hydrogen and oxygen are produced. The TEG is present in the system to recover any wasted heat from the gas turbine. A diagram for this process is given in Figure 6.

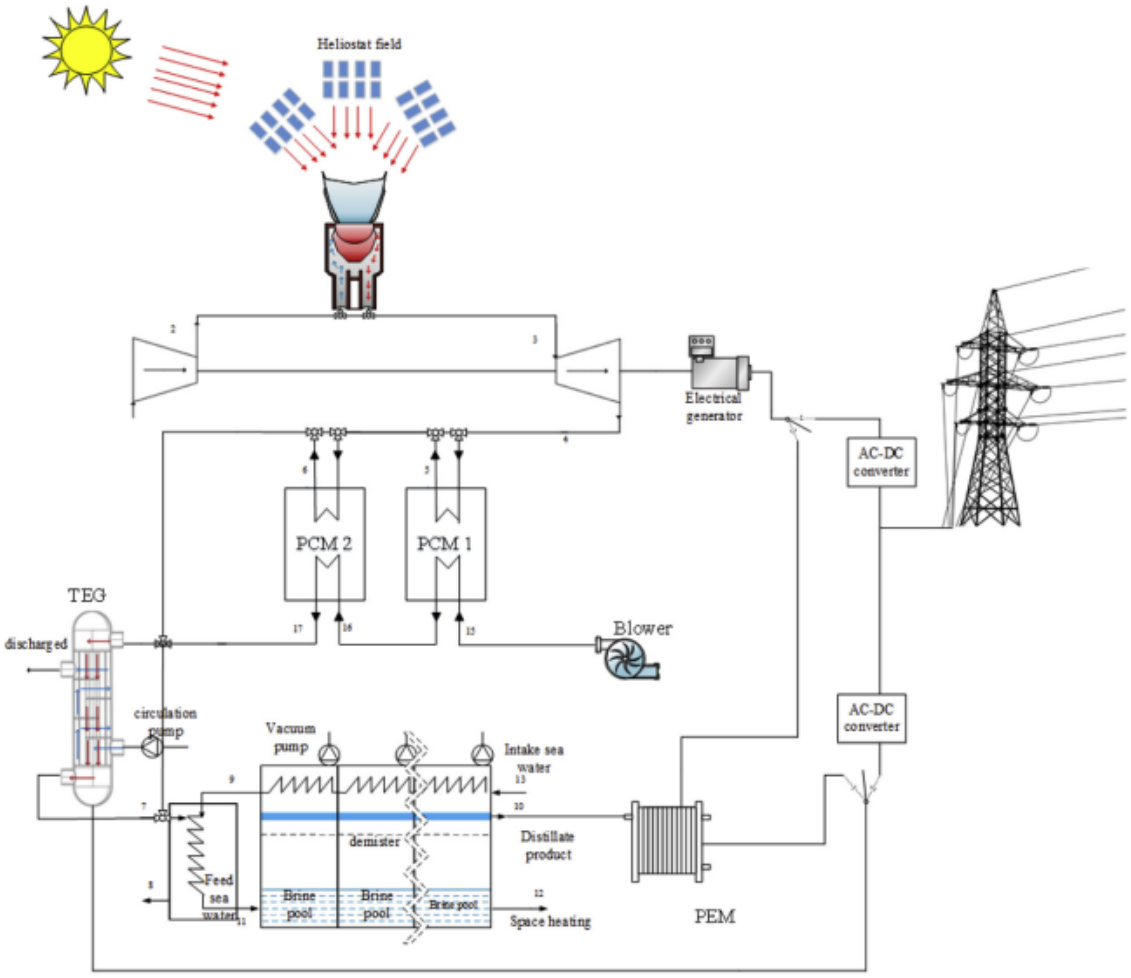

Figure 6 - Diagram of process designed by Demir and Dincer for hydrogen production from seawater [35].

This system described above was analysed by Demir and Dincer to find the overall energy and exergy efficiencies of the system, as well as the theoretical hydrogen, electricity and desalinated water production rates. They also investigated the impact that solar irradiation level, wind speed and the operating temperature of the electrolyser had on the system. To achieve this, a COMSOL Multiphysics software package was used to analyse the TEG unit and all other units were analysed using Engineering Equation Solver (EES). The results obtained showed that the overall energy efficiency of the system was 42.5% and the hydrogen production rate was 129.9 kg per day. In addition to this, it was shown that if the temperature of the PEM electrolyser was increased from 8.9^{o}C to 80.0^{o}C, the hydrogen production rate could increase by 23.5 kg/day. However, as previously mentioned, the analysis on this system was carried out so that only excess electricity (above 2.5 MW) was used for electrolysis; the hydrogen production rate could theoretically be much higher is all of the electricity was used for this purpose.

Although this system benefits from producing valuable desalinated water, disposing of the high-salinity brine could become an issue, especially if the system is intended for offshore use. In this scenario, the desalinated water that is discharged from the electrolysis stage may need to be used to restore the brine to typical seawater salinity so that it can be discharged to the sea.

Delpisheh et al have proposed a system which combines the organic Rankine cycle (ORC) with a desalination unit and a PEM electrolyser to produce hydrogen, oxygen and desalinated water [36]. The system was analysed in three different modes: low solar radiation (solar mode), high solar radiation (solar and storage mode) and no solar radiation (storage mode). A schematic for this system is given in Figure 7. The ORC is powered by thermal energy collected from parabolic trough solar collectors (PTSC) which is used to heat therminol-66 heat transfer fluid. This section is referred to as the solar subsystem and contains two thermal storage tanks (cold storage and hot storage) to be used to store energy when solar radiation is high, i.e. in solar and storage mode. The thermal energy is then transferred via a heat exchanger to the ORC working fluid, n-octane. The working fluid then enters a turbine where it produces electricity using a generator, which can be used to power the downstream PEM electrolyser. Using a multi-heat recovery system, the n-octane is then cooled before entering the ORC pump. By utilising waste heat at this stage instead of employing a cooling tower, energy can be saved and the efficiency of the process is improved. The heat recovered from the n-octane stream is then conveyed to a humidification dehumidification (HDH)-based desalination cycle, where seawater is prepared to be fed into the PEM electrolyser. The desalinated water enters the electrolyser at the operating temperature, after being heated in HX-1. The proposed design of the HDH-system is based on work by Sharqawy et al, which investigates the optimal set-up for these types of systems, maximising utilisation of thermal input [37].

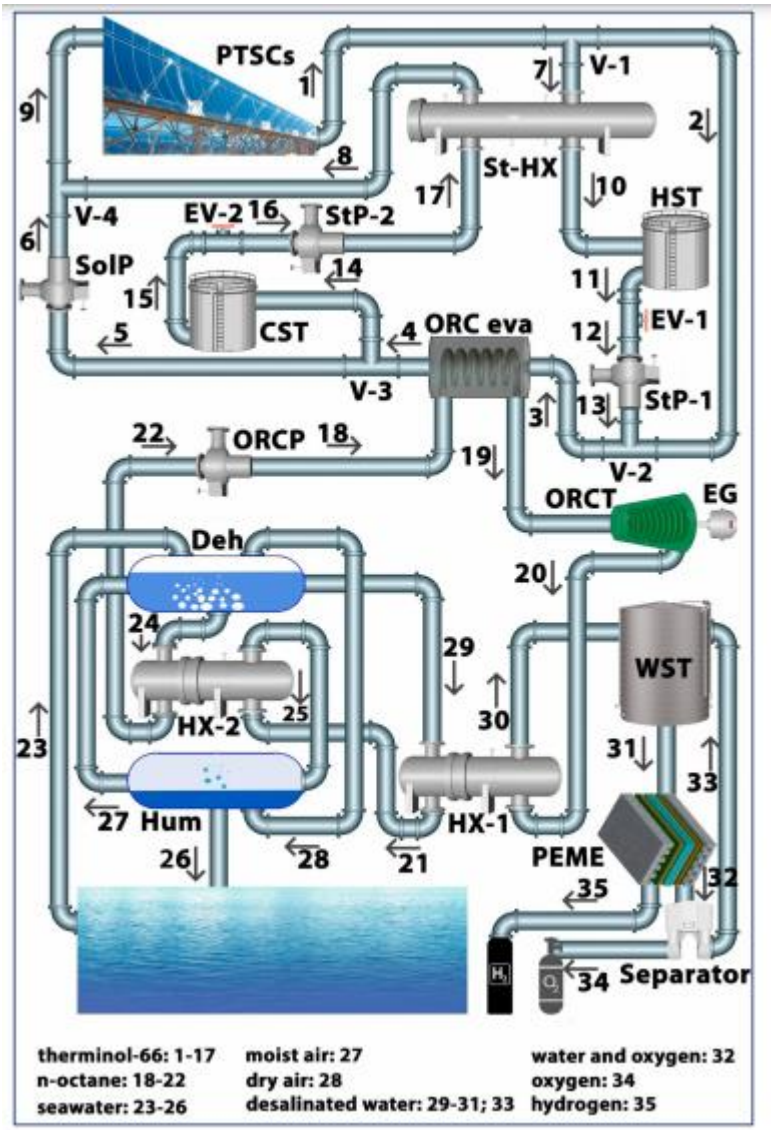

Figure 7 - Process flow diagram for process described by Delpisheh et al for producing hydrogen from seawater [36].

In this parametric study, a simulation of the energy system described above was carried out using EES software and optimised using a genetic algorithm (GA) method. For the low, high and no solar irradiation modes, the respective hydrogen production rates prior to optimisation were found to be 4.33 g/s, 2.62 g/s and 3.54 g/s based on desalinated water flowrates of 1.91 kg/s, 1.06 kg/s and 1.51 kg/s to the PEM electrolyser. The corresponding thermal energy efficiencies for the overall system based on these production rates were 81.46%, 27.73% and 50.61%. Following optimisation, the maximum hydrogen production rates were found to be 4.97 g/s, 3.95 kg/s and 4.23 kg/s, respectively, for the three modes and the maximum efficiencies were 85.68%, 38.65% and 54.14%.

This system is designed for use in coastal areas as it can be used to simultaneously produce both desalinated water and hydrogen; the energy collected in the PTSC may be more than what

is required to desalinate the maximum flowrate of water into the PEM electrolyser stack, meaning there will be excess desalinated water produced. However, as with the previously discussed system proposed by Demir and Dincer, the brine stream that is produced post-desalination will likely have too high a salinity to be disposed to the sea safely, which creates an issue of disposal. Furthermore, the use of hydrocarbon-based heat-transfer fluids is undesirable as these are derived from non-renewable fossil fuel sources.

A system of similar principles was explored by Siddiqui and Dincer [38]. A concentrating solar power system is integrated with an ORC, a reverse osmosis (RO) desalination unit and a PEM electrolyser to produce desalinated water, hydrogen and electricity. Figure 8 depicts the set up of the process. The solar subsystem operates in a similar fashion to the previously described process created by Delpisheh et al. The desalination unit is designed based on a prior study by El-Emam and Dincer [39]. Seawater is pumped into a cartridge filter where suspended particles are removed. The saline water is then prepared for reverse osmosis by being passed through a mixer for chemical pre-treatment, which prevents damage to the RO membrane elements. The fluid leaving the chemical pre-treatment stage is then pressurised before entering the RO stage, where a pressure loss is experienced (60 bar to 51 bar). The output stream from this stage then enters the PEM electrolyser. The overall energy efficiency of this system was found to be 23.2%.

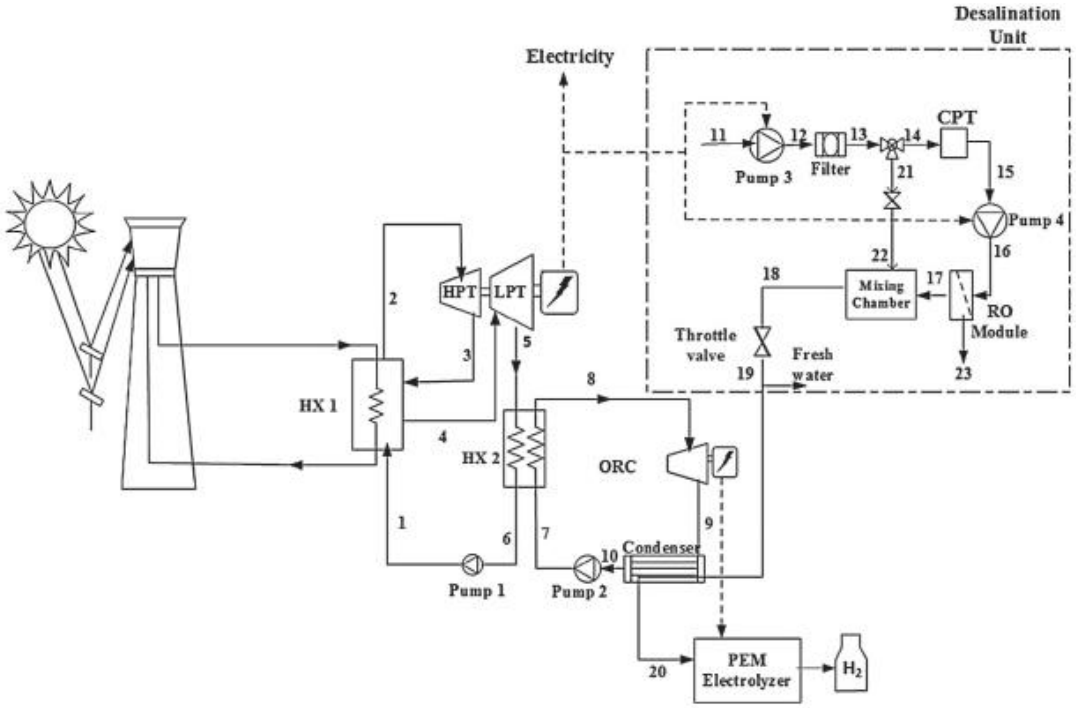

Figure 8 - Diagram of process described by Siddiqui and Dincer for producing hydrogen from seawater.

Although a novel and interesting set-up, the salinity of the feed entering the PEM electrolyser in this process is 350 ppm, which is above the threshold TDS for PEM electrolysers. Therefore, for this process to be feasible, another filtration unit would have to be added, such as distillation or HDH.

Kumari et al investigated the potential for producing hydrogen through electrolysis of seawater vapour [40]. The principle of this investigation was that because seawater vapour is free of the contaminants present in liquid seawater, it could be used in a PEM electrolyser without breaching the maximum TDS limit. In this system, seawater-humidified air at 80% relative humidity (RH80) was fed to the anode of the PEM electrolyser while dry nitrogen gas (RH0) was fed to the cathode as a carrier gas. Air at this humidity was selected because this is the global average ambient humidity level of air above sea and so, if used offshore with seawater, air would not have to be pre-humidified before entering the electrolyser. Post-electrolysis, air and oxygen leave the PEM cell at the anode and nitrogen and hydrogen leave the cell at the cathode. The use of photovoltaics (PVs) to provide electricity to the electrolyser was also investigated in this work.

The system was tested using both deionised water vapour and seawater vapour. It was shown that the current density stayed relatively stable at around 10 mA/cm^2 for both feedstocks for over 40 h. It was also found that increasing the flowrate of feedstock gases to the electrolyser

cell increased the maximum current density that could be achieved. This is because the polymer membrane material, Nafion®, only maintains its high ionic conductivity when hydrated to a certain level; increasing the flowrate of humidified air increases the flowrate of water vapour and therefore the ionic conductivity of the polymer. The system was tested using air at various humidity levels to determine the impact on electrolyser performance. Intuitively, the maximum current density achieved also increased with increasing relative humidity.

Although this proposed technique benefits from being relatively simple with few stages, the product gases that are produced exit the electrolyser mixed with other gases, as opposed to the previous systems where they were either mixed with water or a liquid alkaline solution. This will make separation of the product gases more difficult.

2.2 Seawater Electrolysis Using Membrane-less Devices

The use of an electrolyser cell without a membrane presents many benefits. Reactor lifetime is increased because the issue of membrane pores becoming clogged is removed. The simplicity of the design of membrane-less electrolysers means manufacturing becomes simpler; many researchers have seen success in creating 3D-printed prototype membrane-less electrolysers. Furthermore, costs are reduced significantly, due to the fact that commonly used membrane materials, such as Nafion®, tend to be costly. Additionally, liquid electrolytes have ionic conductivities that surpass those of solid polymer electrolytes, which leads to higher efficiency of the cell.

Research conducted into this field showed that most membrane-less electrolysers currently being investigated are microfluidic devices. This is mainly because by minimising the electrode separation distance, solution resistance is also minimised and electrolysis efficiency increases. Microfluidic devices are roughly defined as having a channel diameter that is in the micron range whereas millifluidic channels are in the millimetre range [41].

A novel, membrane-less electrolyser design was proposed by Hashemi et al in 2015 [42]. This electrolyser consists of a microchannel (105 μm electrode distance) with parallel electrodes upstream of a T-junction which separates products, as shown in Figure 9. The separation of products in this device is achieved through closely controlling the fluid mechanic forces in the channel by taking advantage of the Segré-Silberberg effect. Experimental testing of the device showed that a current density of over 300 mA/cm^2 was achieved at a voltage of 2.6 V when using 1 M H_2SO_4 as an electrolyte. Additionally, product cross-over was as low as 0.4% when using an electrolyte flowrate of 14 mL/h at a current density of 71.5 mA/cm^2. However, for

flowrates of less than 11 mL/h, the cross-over experienced surpassed the acceptable limit; the maximum threshold for oxygen in hydrogen is 4% - anything above this becomes hazardous [43]. The research group found that higher flowrates yielded better separation of products, due to less coalescence of gas bubbles occurring.

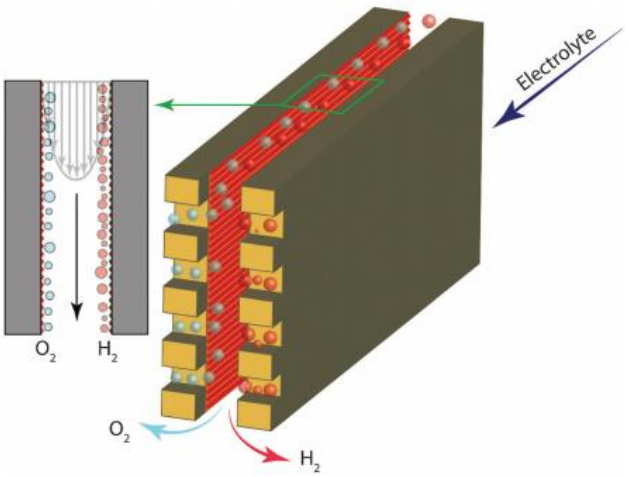

Figure 9 - Depiction of membrane-less electrolyser device designed and tested by Hashemi et al [42].

Although only tested at a lab-scale, this device could be scaled up for industrial production by stacking large parallel plates on top of each other, all with the same inter-electrode distance. However, this particular study only tested the device using fresh water plus electrolyte as the input, so further testing would be required to determine its performance when using seawater. A patent was filed for this electrolyser in 2015 and approved in 2021 [44].

Another concept for a membrane-less electrolyser was developed in 2015 by Gillespie et al [45]. This electrolyser was constructed with an inter-electrode gap of 2.5 mm, making it a millifluidic device. The divergent electrode-flow-through (DEFT) design features two circular mesh electrodes opposite and parallel to each other, through which electrolyte flows. Gas produced at surface of electrode is swept into corresponding stream by the electrolytic flow, creating separation of the products. The device was tested under various conditions and it was found that lower flow velocities resulted in lower efficiencies due to gas meniscuses forming on the cathode and anode, which increased the resistance of the solution. Therefore, a flowrate between 0.075 ms^{-1} and 1.5 ms^{-1} was recommended to optimise between efficiency and pumping power. Furthermore, it was concluded that for lower velocities, a smaller electrode gap is preferred as this increases field intensity and therefore electrical efficiency but for higher velocities, a larger electrode gap is required due to the formation of bubbles in the flow.

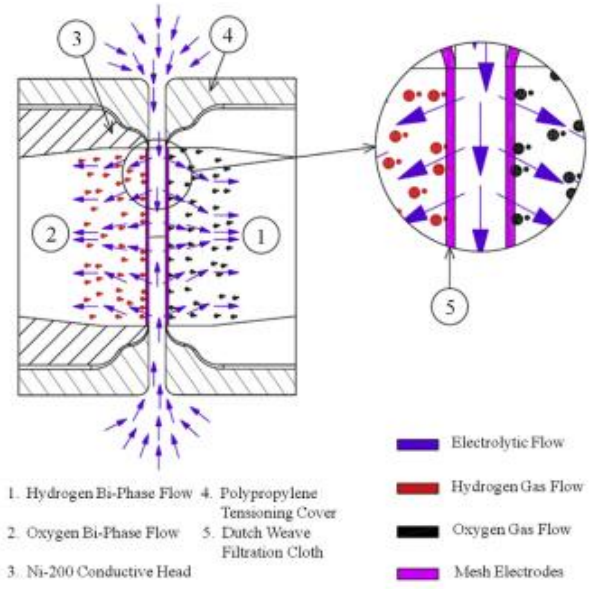

Figure 10 - Diagram of membrane-less electrolyser designed by Gillespie et al, showing material flows [45].

Tests carried out on this device showed that a hydrogen purity as high as 99.83% could be achieved under certain conditions. A current density of 474.4 mA/cm^2 was reached at a cell voltage of 2 V. It was also shown that this technology can accommodate fluctuating power sources and would therefore be compatible with renewable, intermittent power sources such as wind and solar power. However, the device was tested as an alkaline electrolyser using 30 wt% KOH as the electrolyte and so the performance of this device when electrolysing seawater is unknown. An international patent for this device was granted in 2013 [46].

In 2016, a paper was published by O'Neil et al detailing an electrolyser cell design also with mesh flow-through electrodes [47]. Whereas in the previously discussed devices the electrodes were either parallel or perpendicular to the flow, this device contains electrodes that are at an oblique angle to the flow. This provides benefits in comparison to other devices as angular electrodes may be more easily integrated into a single-component device. Furthermore, because this device uses a rectangular channel, it is claimed that scaling up the device will be easier than it would with a device which uses circular electrodes with annular flow. However, using a rectangular channel creates a more complicated flow pattern, in which some of the fluid can potentially remain stagnant [48]. This makes the tube walls more susceptible to corrosion and build-up of contaminants.

Negatively charged ions in the electrolyte flow are attracted to the anode where oxygen gas is produced and positively charged ions are attracted to the cathode where hydrogen gas is

produced. There is a thin divider placed between the anode effluent and the cathode effluent to separate the product gases. A drawing of the device is given in Figure 11.

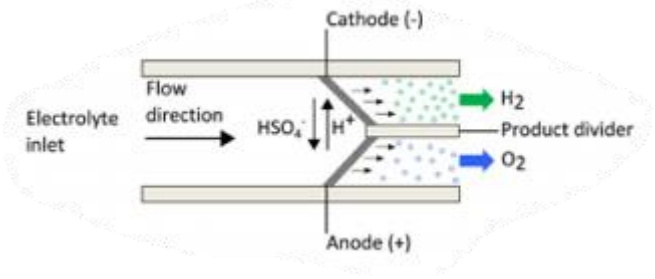

Figure 11 - Two-dimensional depiction of membrane-less device created by O'Neil et al showing flow direction of materials [47].

This angle of separation between electrodes was varied from 30^o to 180^o throughout testing so that its impact on electrolyser performance could be evaluated, but channel width was kept constant throughout. Increasing the angle of separation was found to increase the solution resistance and therefore efficiency. The absolute current was found to decrease with increasing angle of separation, but the current density remained the same due to the change in electrode area. The highest current density was achieved using 1 M KOH (~220 mA/cm^2 at 2.5 V) but was also found for 0.5 M H_2SO_4 (~150 mA/cm^2 at 2.5 V). The maximum product cross-over experienced was 2.8% at a current density of 100 mA/cm^2 and a flow velocity of 26.5 cm/s. The cross-over was only tested at an electrode separation angle of 30^o, but this was expected to be when the highest cross-over was experienced due to the acute angles. It was found that high current densities and moderate flowrates can help to minimise dissolution of products in the aqueous phase.

The same research group published released further research on a similar device in 2017 [49]. The device, pictured in Figure 12, differs to the previous device in that electrodes are positioned perpendicular to the flow. Furthermore, a pH gradient is induced in the channel when electrolysing brine, which creates an alkaline cathode effluent containing hydrogen gas bubbles and an acidic anode effluent containing oxygen gas bubbles. The device was tested using various electrolytes and it was found that using brine as an electrolyte created a greater overpotential, and therefore a lower voltage efficiency, in comparison to other electrolytes. The electrical input required to the device was found to be 40 kWh/kmol of product formed at a current density of 100 mA/cm^2 and the current utilisation (also referred to as Faradaic efficiency) varied between 50% and 87%.

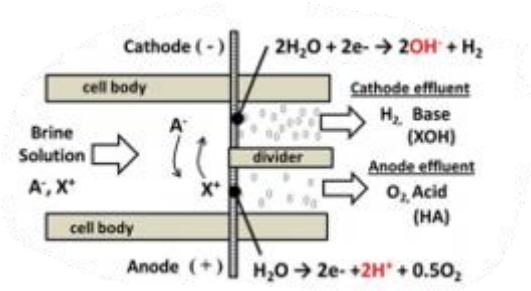

Figure 12 - Diagram showing electrolyser device designed by O'Neil et al which shows operating principles and product streams [49].

This research found that the use of a flowing electrolyte is essential when using this device, as stagnant flow creates a higher product cross-over. Furthermore, the flowrate of the electrolyte is critical because the rate of dilution of the products depends on it. It was also found that, by varying the current density and voltage applied to the electrolyser, the pH of each effluent stream could be controlled, shown in Figure. A patent was filed in 2016 for the devices discussed shown in Figures 11 and 12. The patent, which was filed by Esposito and O'Neil, was approved in 2020 and describes the many possible functions and architectures of the device.

In 2017, Rarotra et al presented three different configurations of a simple membrane-less electrolyser design which separate gaseous products from electrolysis [50]. These configurations are shown in Figure 13. The first is a straight-channelled device without a separator, the second a straight-channelled device but with a separator and the third a Y-shaped device with a separator. Again, the devices are all microfluidic (channel diameter was 50 μm). In this case, the electrode gap tested was 10 mm but field intensity and therefore efficiency could potentially be improved by decreasing this. The device was tested using seawater and it was found that hydrogen bubbles began to form at an applied potential of around 2 V. The volume of hydrogen produced was found to increase almost linearly with applied voltage and with flowrate of electrolyte into the device. Separation efficiency also increased (and therefore product cross-over decreased) with increasing voltage. However, there was little information given regarding current densities and cell voltages achieved when testing the device. A patent was filed for this device in 2017 and approved in 2021.

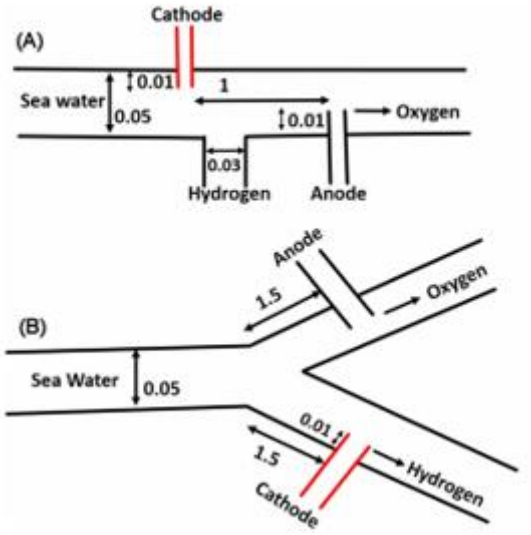

Figure 13 - Two configurations of the electrolyser design proposed by Rarotra et al for electrolysis of seawater [50].

A system in which a floating, membrane-less electrolyser was used in conjunction with PV panels was proposed in 2018 by Davis et al [51]. The electrolyser used in this design was like previous devices in that it contained mesh, flow-through electrodes, but differed in that the electrodes were positioned vertically rather than horizontally. The electrodes are asymmetrical, in that they are only coated in electrocatalyst material on one side, which is intended to minimise product cross-over by constraining gas nucleation to the outer face of the electrode. These electrodes induce the formation of hydrogen and oxygen gas bubbles which are then separated into two collection chambers based on buoyancy. It is proposed that floating PV panels are fitted above these collection chambers which can then provide electricity to power the electrolysis. The design is shown in Figure 14.

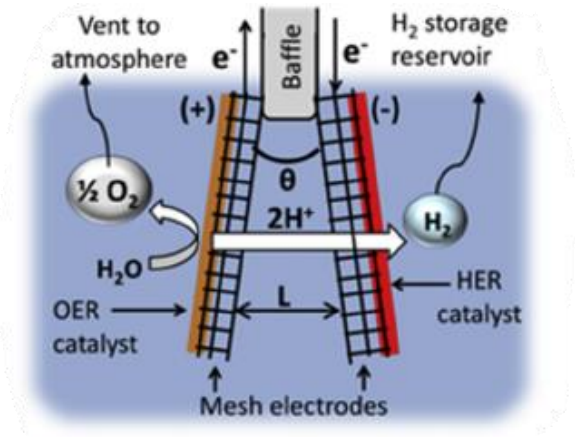

Figure 14 - Design proposed by Davis et al for electrolysing seawater using asymmetric electrodes [51].

Also in contrast to previously described devices, this device was intended for use with a stagnant electrolyte rather than flowing and could therefore be submerged directly into seawater with no pumping of electrolyte required, reducing overall energy requirements of the system. On testing the impact of using asymmetrical electrodes, it was found that this configuration gave lower product cross-over as expected (1% compared to 7% for symmetrical at 100 mA/cm^2). However, symmetrical electrodes gave a slighting higher electrolysis efficiency (53.4% compared to 50.6% for asymmetrical electrodes at 100 mA/cm^2); this is due to there being a larger active surface area available for reaction in the symmetrical electrodes.

The angle of separation between electrodes was varied so that the impact of this parameter could be determined. It was found that by increasing the separation angle and therefore the electrode separation distance, electrolysis efficiency decreased due to the increase in solution resistance. However, product cross-over was found to decrease on increasing the angle of separation, due to there being a greater spatial separation between the products. Furthermore, increasing current density also decreased product cross-over, because there is a lower incidence of gases dissolving into the aqueous phase than there is with lower current densities. This device was tested using saline water (0.6 M NaCl) as the electrolyte and as with other devices, it was found that this required a greater overpotential than when using other electrolytes (3.68 V at 100 mA/cm^2 compared to 2.44 V when using 0.5 M H_2SO_4 as the electrolyte). Because this device was only tested using NaCl solution and not seawater, it is difficult to predict whether other ions present in seawater would have an impact on the performance.

A 3D-printed millifluidic electrolyser cell was presented in 2019 by Hashemi et al [52]. A photo of the prototype electrolyser is given in Figure 15. The device consists of a single electrolyte stream with a cathode and anode which are parallel to the flow and a Y-junction separator. Product gas bubbles form on the electrode surface and are swept into the corresponding channel by the flowing electrolyte. Inertial fluidic forces within the device are manipulated to control flow within the device and product separation. The formation and coalescence of bubbles during electrolysis in membrane-less electrolyser designs can inhibit performance of the cell by creating violent flow regimes, which is why microfluidic channels are normally preferential. However, this study investigates the use of a millifluidic device with a channel diameter of 1 mm at Reynolds numbers of up to 312.

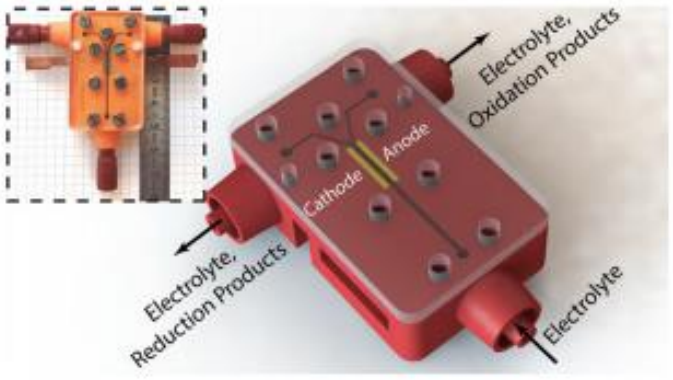

Figure 15 - Illustration of electrolyser device designed by Hashemi et al with photo of 3D printed prototype in top left corner [52].

The electrolyser was tested using 20 wt% NaCl as an electrolyte, which is almost 6 times the salinity of seawater and therefore more conductive. Therefore, the results produced when using seawater could not be expected to be as positive as those found using this brine as an electrolyte. Current densities of up to 706 mA/cm^2 were achieved at a voltage of 3.25 V, which the authors claim to be similar to the performance of an industrial membraned electrolyser. However, as stated in Table 1, some electrolysers are capable of achieving current densities of up to 2000 mA/cm^2 at a cell voltage of only 2.2 V [9]. The current density was found to increase to 706 mA/cm^2 from 593 mA/cm^2 by increasing the flowrate of electrolyte from 300 mL/h to 1200 mL/h. This is because by increasing the flowrate, larger drag forces are exerted on the product bubbles which are formed on the electrode, meaning that they are detached from the electrode and moved upstream at a smaller bubble size.

A patent was filed in 2014 for a portable water electrolysis device that claims to be able to electrolyse undistilled water without using a liquid electrolyte [53]. The device, pictured in Figure 16, splits water into hydrogen and oxygen through a series of anode rods and hexagonal cathode matrices. The hydrogen gas produced is separated from oxygen by passing through tube walls which are permeable to hydrogen but not oxygen. The inventor claims benefits of this electrolyser such as it being portable but also scalable for industrial applications. This electrolyser is being commercialised by Gilman Industries as Evolve^{TM} C-37 and it is claimed by their website that the device is able to work with tap water, wastewater and seawater. Purity tests by Rensselaer Polytechnic Institute - Center for Future Energy Systems found that when electrolysing tap water, hydrogen purity of up 99.32% was observed [54]. However, other than this, there is little information available on the performance of the electrolyser cell in terms of efficiencies or current densities.

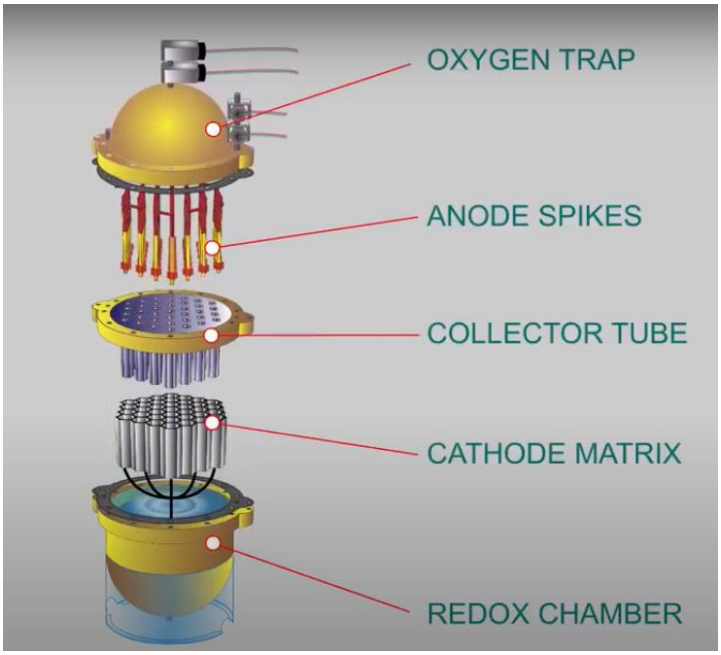

Figure 16 - Illustration showing components of interior of Evolve™ C-37 Electrolyse patented by Gilman Industries, taken from [55].

The simple but effective design of all of these membrane-less electrolyser cells make them promising technologies for direct seawater electrolysis. However, these have mostly only been tested at a lab-scale and are not yet ready for mass deployment. Furthermore, they must be tested using real seawater as opposed to simulated seawater to prove their performance ability; real seawater will contain many more contaminants other than dissolved ions that can inhibit performance of the electrolyser through scaling and biofouling.

2.3 Electrocatalysts for Seawater Electrolysis

Due to the possibility of chlorine forming during seawater electrolysis, a major focus area in the field is developing electrocatalysts which promote OER over the competing ClER. Furthermore, due to the high salinity content of seawater, electrocatalysts are required that can withstand the harsh environment without being corroded or without precipitation of harmful compounds occurring on the electrode.

A review of the literature available on ‘recent advances in seawater electrolysis’ was recently conducted by Mohammed-Ibrahim and Moussab [17]. They found that highly OER selective electrocatalysts include transition metal hexacyanometallates based electrocatalysts, transition metal nitride and layered double hydroxide (LDH) integrated with transition metal sulfide, with some proving long term stability of over 600 hours. They also investigated electrocatalyst

materials which improve HER. A summary of the findings on OER selective electrocatalysts is given in Table 3.

Table 3 - Results on stability and durability of various OER electrocatalysts, recreated from [17].

OER Catalysts	Electrolyte	Durability (h)	Remark after stability test	Reference
Cellular stainless steel	1 M KOH + 0.6 M NaCl	110	Negligible decay at 40 mA/cm^2	[56]
NiCo	Seawater	~40	98.83% retention at overpotential of 270 mV	[57]
PtPd	Seawater	~12	Negligible decay	[58]
PtFe	Seawater	12	Reasonable stability	[58]
PtCo	Seawater	~11	Reasonable stability	[58]
PtNi	Seawater	~10	Negligible decay	[58]
CoFe LDH	Simulated seawater	8	~86% retention at overpotential of 560 mV	[59]
NiFe LDH/C	0.1 M KOH + 0.5 M NaCl	2	Reasonable stability at 10 mA/cm^2	[11]

Although a review on seawater electrolysis for hydrogen production, the paper by Mohammed-Ibrahim and Moussab differed to this one in that it focussed primarily on advances in electrocatalyst materials and did not cover novel technologies or processes for electrolysing seawater. Because this paper already gives a highly detailed review on this subject, the information given on electrocatalysts in this paper will be limited to this section.

2.4 Software Review

Various software packages were investigated to assess their applicability for analysing seawater electrolysis processes. Aspen Plus from Aspen Technology™ was identified as being suitable due to its capabilities in simulating chemical processes and creating custom unit operation models. This feature could have been utilised for processes featuring non-standard electrolysers, such as the membrane-less electrolysers described previously. Furthermore, the author was already familiar with this software which made it more appealing.

Although the software was available through the University of Strathclyde server, technical issues meant that the package was not able to be accessed when using a PC off campus. Due to the ongoing COVID-19 pandemic, it was not possible to use a PC on campus. Therefore, the decision was made to explore other software programs.

ChemCAD from Chemstations™, another chemical process simulation software, was investigated due to its similarity to Aspen [60]. However, it was discovered that this program

was not available to download for student access. Another process simulation software package from the CAPE-OPEN project called COCO was identified [61]. Although this program was free to download and easy to use, its capabilities were limited and seemed to be more focused on oil and gas applications, as the only chemical components that could be simulated were mostly hydrocarbons, making it unsuitable for this project.

It was therefore decided that any calculations involved in the analysis section of this project would be carried out using Microsoft Excel. This would allow for more flexibility in adjusting certain parameters throughout the project and a better understanding of the numerical aspect of the analysis.

3.0 Methodology

The following sections detail the procedure carried out to achieve the aims that were set out in Section 1.3.

3.1 Processes for Hydrogen Production from Seawater

Four different methods for producing hydrogen using seawater electrolysis were identified based on processes that were discussed in Sections 2.1 and 2.2. Process flow diagrams, mass balances and energy balances were created for each of the four processes. Power consumption of equipment involved in the processes such as compressors or pumps was also taken into consideration.

The four processes selected were as follows:

1. Alkaline electrolysis of with NaCl precipitation
2. PEM electrolysis using SW vapour
3. PEM electrolysis with HDH-based desalination
4. Membrane-less electrolysis with solid SiO_2 and $Mg(OH)_2$ as by-products

The processes will henceforth be referred to as Process 1 (Alkaline), Process 2 (PEM 1), Process 3 (PEM 2) and Process 4 (Membrane-less), respectively. Seawater (SW) was used as the feed for all four processes and the assumed composition is given in Table 4.

Table 4 - Typical concentrations of various ions found in seawater [33].

Ion	MW (g/mol)	Concentration (mg/L)	Concentration (mol/L)
Chloride, Cl^-	35.453	18980	0.535
Sodium, Na^+	22.990	10556	0.459
Sulfate, SO_4^{2-}	96.060	2649	0.028
Magnesium, Mg^{2+}	24.305	1262	0.052
Calcium, Ca^{2+}	40.078	400	0.010
Potassium, K^+	39.098	380	0.010
Bicarbonate, HCO^{3-}	61.017	140	0.002
Strontium, Sr^{2+}	87.620	13	0.000
Bromide, Br^-	79.904	65	0.001
Borate, BO_3^{3-}	58.810	26	0.000
Total dissolved solids (TDS)		**34471**	

For the purpose of this project, it is assumed that the processes will be used to produce hydrogen from seawater on an offshore unit in the North Sea of Scotland. Therefore, the temperature of the seawater feed was assumed to be 5ºC, based on a minimum average temperature experienced in this sea [62]. The minimum temperature was chosen so that the calculated thermal input to the processes would be a maximum. The temperature of the air above the sea was also assumed to be 5ºC [63].

3.2 Process Descriptions and Flow Diagrams

A full description of the operation of each of the four processes identified is given in the following sections, along with a process flow diagram for each.

3.2.1 Process 1 (Alkaline) Process Description

The process flow diagram for this process given in Figure 18 was created based on the method devised by Amikam et al which was discussed in Section 2.1.1. [13]. Seawater enters S100 and is pumped through centrifugal pump CP-100 where it is increased in pressure from atmosphere pressure (1.01 bara) to 15.01 bara in preparation for entering the nanofiltration (NF) unit, F-100. The stream is passed through heat exchanger HX-100 and raised in temperature to 25ºC from 5ºC using low pressure (LP) steam. The operating temperature and trans-membrane pressure of F-100 (25ºC and 14 bar) were selected based on work done by Telzhensky et al [64]. Stream S200 contains ions rejected during the NF process such as Mg^{2+} and Ca^{2+} and

90% of the water input to the unit (based on 10% water recovery [13]). The remaining 10% of the water and most of the Na^+ and Cl^- ions are exit F-100 at atmospheric pressure in S300.

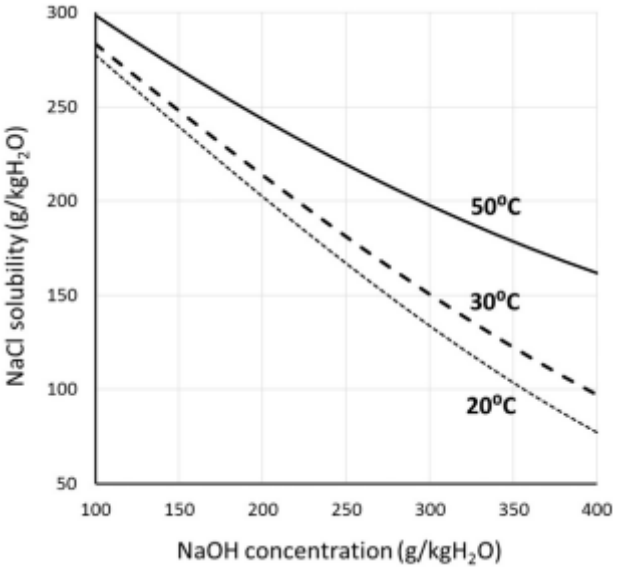

Figure 17 - Graph showing NaCl solubility in water as a function of NaOH concentration at varying temperatures, taken from [13].

The stream then enters settling tank T-100 where precipitation of NaCl salt occurs based on Equation 11. The principle of this reaction is based on the common ion effect; the sodium hydroxide (NaOH) concentration and temperature are maintained so that the solubility of NaCl in water is low and therefore the salt begins to precipitate. A temperature of 25°C and a NaOH concentration of 400 g/kgH_2O were selected so that maximum precipitation can occur without having to cool the stream post-nanofiltration. The solubility of NaCl in these conditions are shown in Figure 17.

$$Na^+(aq) + Cl^-(aq) \rightarrow NaCl(s) \qquad (11)$$

Solid NaCl is rejected in S400 and an alkaline solution exits T-100 in S500. This stream then enters the electrolyser AE-100 where it is electrolysed into gaseous oxygen and hydrogen based on the reaction in Equation 7. Oxygen exits in S700 and is compressed to 200 bar in C-100 before being storage in T-200 and hydrogen is compressed to 350 bar in C-200 then stored in T-300. The alkaline solution which is unused during the electrolysis process exits AE-100 in S600, where it is cooled back to 25°C before being recycled to T-100.

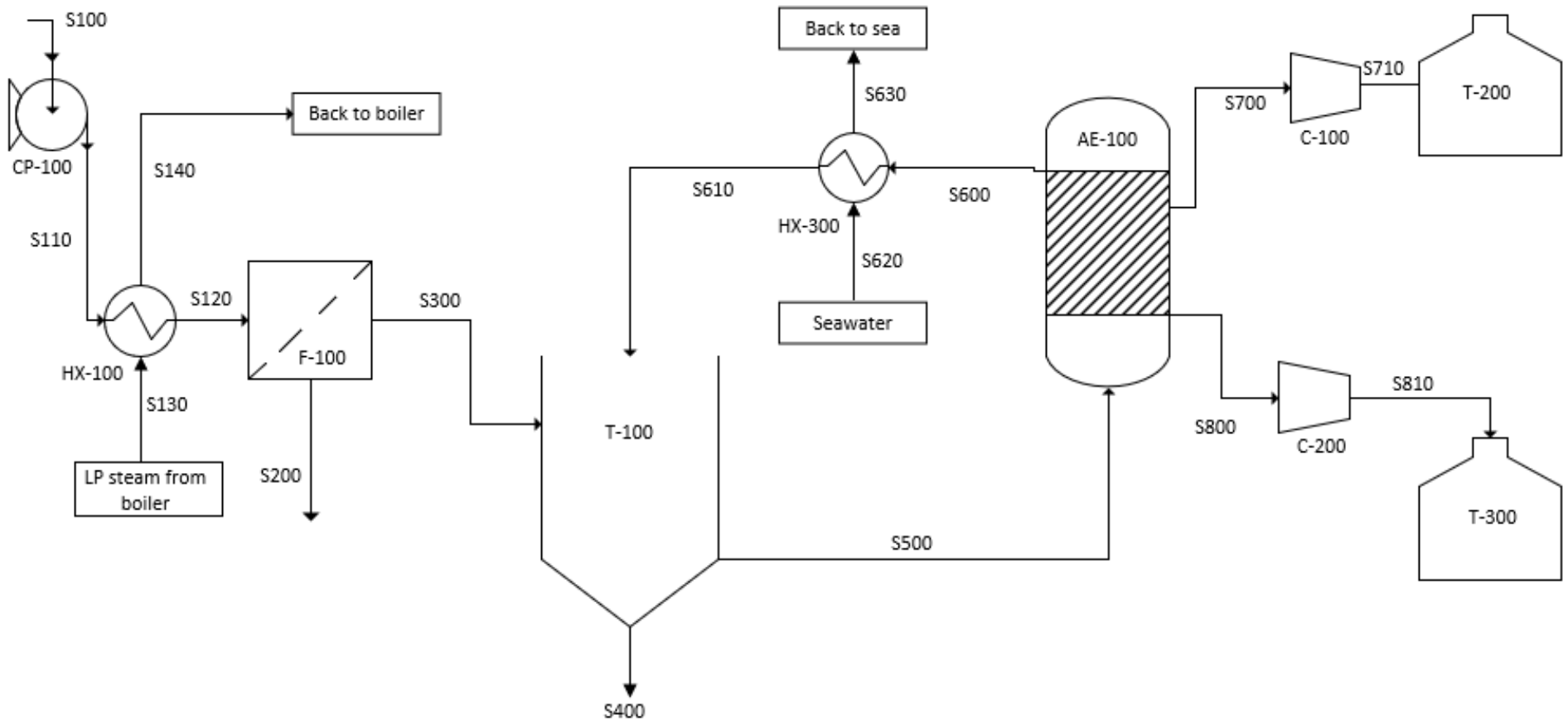

Figure 18 - Process flow diagram for Process 1 (Alkaline).

3.2.2 Process 2 (PEM 1) Process Description

This process was partly based on the process described by Kumari et al discussed in Section 2.1.2 with an added pressure swing adsorption (PSA) unit to separate hydrogen gas from nitrogen. Although the process by Kumari et al operates with air at RH80, it was decided to humidify the air to RH100 to ensure that the polymer membrane of the PEM electrolyser stays sufficiently hydrated and therefore maximise efficiency [40]. A process flow diagram is given in Figure 19. Seawater enters S100 and is pumped using centrifugal pump CP-100 into H-100 where it is used to humidify air feed stream S120. This stream enters H-100 at 80% relative humidity (RH80) and is humidified to RH100 and heated to 80^{o}C within H-100. The humified air leaves at atmospheric pressure in S300 and enters electrolyser PEM-100 at the anode. Excess SW leaves H-100 in S200 and is mixed with recycled, unreacted water stream S510 to restore salinity to its initial value in S100. This mixed stream is then cooled in HX-100 to a minimum of 8^{o}C (maximum $\Delta T = 3^{o}C$, inlet $T = 5^{o}C$) before being discharged back to the sea.

Dry nitrogen gas (RH0) enters PEM-100 at the cathode in S400 as a carrier gas. Seawater vapour is electrolysed in PEM-100 based on Equation 10. Air, oxygen gas and unreacted water leave PEM-100 in S500 before being separated in phase separator FD-100. The water exits in S510 and is mixed with S200. Air and oxygen gas leave FD-100 in S520 are expelled to the environment. Nitrogen and hydrogen leave PEM-100 in S600 before entering a PSA unit for separation. The pressure in adsorption columns AC-100 and AC-200 alternates between 30 bar and atmospheric pressure depending on whether they are in adsorption or desorption mode. When the column is operating at 30 bar, i.e. in adsorption mode, gaseous nitrogen is adsorbed by the adsorption material and pure hydrogen leaves the column in S800 before being compressed in C-200 to 350 bar and stored in T-300. While one column is in adsorption mode, flow is restricted to the other column which operates at atmospheric pressure, so that nitrogen is desorbed and exits in S400 before being recycled back to PEM-100.

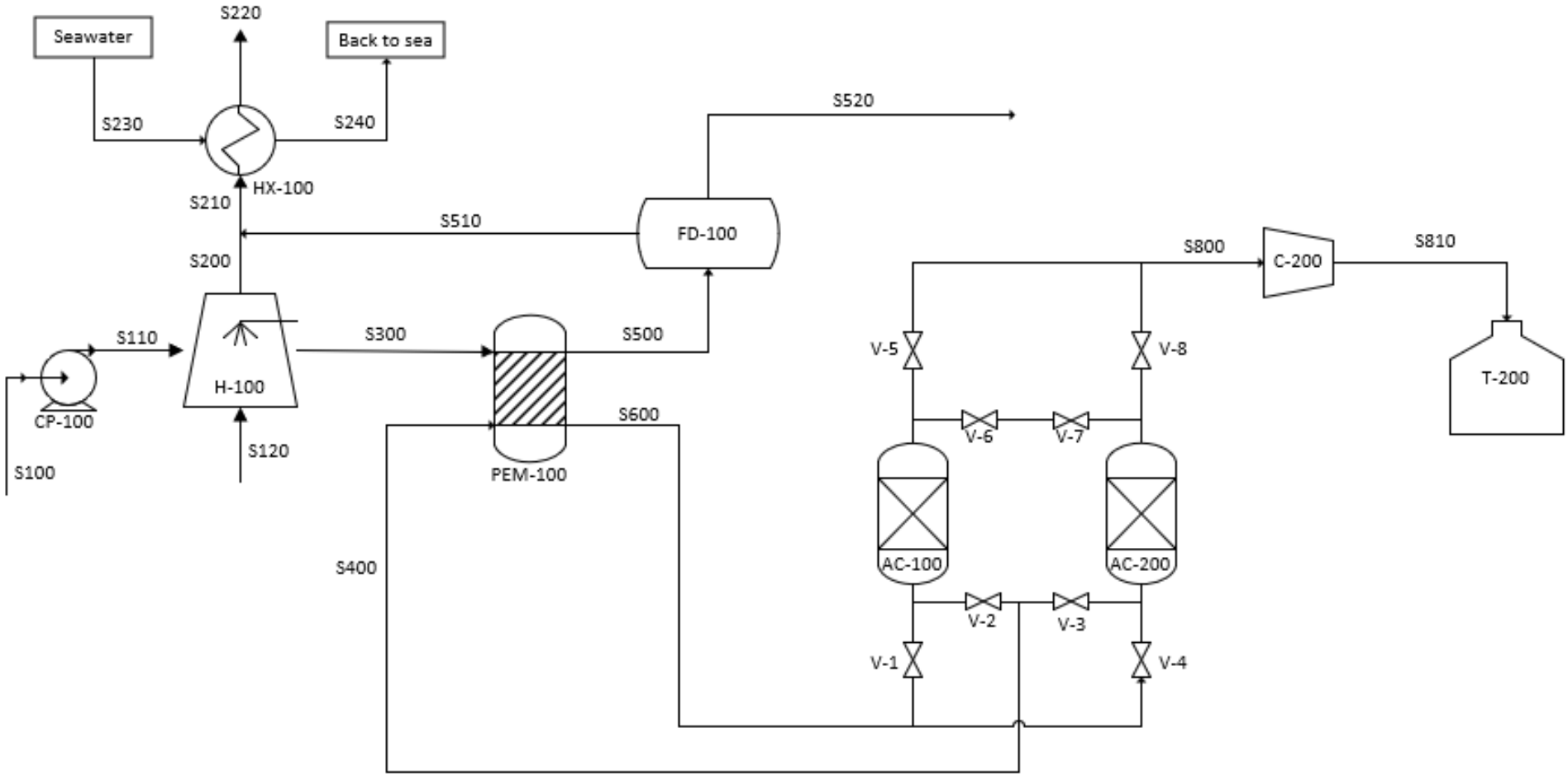

Figure 19 - Process flow diagram for Process 2 (PEM 1).

3.2.3 Process 3 (PEM 2) Process Description

This process is based on a simplified version of the process proposed and analysed by Delpisheh et al [36] which was discussed in Section 2.1.2. Seawater is desalinated using a HDH unit and the pure water is then used in PEM electrolysis.

Seawater enters S100 and is pumped into humidifier H-100 using centrifugal pump CP-100. Dry air (RH0) enters H-100 via S400 and is humidified to RH100. Saturated air leaves H-100 in S300 at atmospheric pressure and 80^{o}C [65]. Seawater with increased salinity leaves H-100 in S200. Saturated air then enters dehumidification unit DH-100 in S300 before being dehumidified to RH0 and recycled back to H-100 in S400. The condensed water from DH-100 leaves in S500 at 80^{o}C and atmospheric pressure and is mixed with recycled post-electrolysis desalinated water to form stream S600. This stream then enters PEM-100 and is electrolysed into product gases hydrogen and oxygen based on Equation 10. Dry hydrogen leaves in S700 at 30 bar and 70^{o}C and is then compressed in C-100 to storage pressure 350 bar before being stored in T-100.

Oxygen gas leaves PEM-100 in S800 along with any unreacted water. The liquid water and gaseous oxygen are then separated in phase separator FD-100. Dry oxygen leaves in S900 before being compressed to 200 bar in C-200 and stored in T-200. The stream of pure water leaving FD-100, S920, is partially recycled back in to be mixed with brine stream S200 so that the salinity of this stream is returned back to initial levels before being discharged to the sea. These two streams combine to form S1000, which is then cooled back to a minimum of 8^{o}C before being discharged. The remainder of S920 is recycled in S930 and mixed with S500 to increase the mass of water entering PEM-100 for electrolysis and therefore increase the mass of product gases formed.

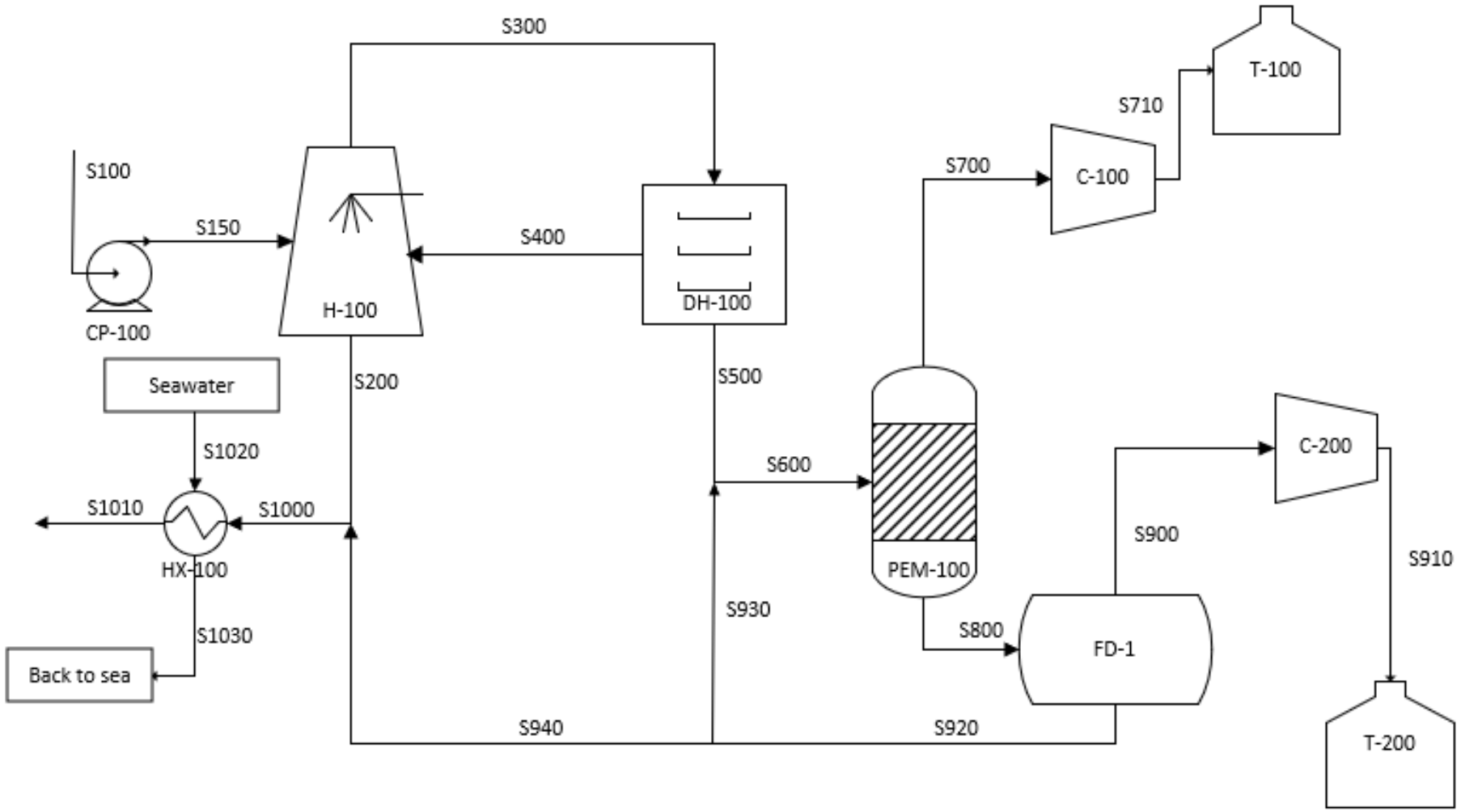

Figure 20 - Process flow diagram for Process 3 (PEM 2).

3.2.4 Process 4 (Membrane-less) Process Description

This process is based on a process which was presented in confidential material provided by sHYp and the membrane-less electrolyser cell discussed in Section 2.2. Two membrane-less electrolysers are used in a direct SW electrolysis system that produces hydrogen, oxygen, magnesium hydroxide ($Mg(OH)_2$) and silicon dioxide (SiO_2).

Seawater is pumped into the system via S100 using centrifugal pump CP-100 before being heated to 20°C in HX-100. The stream then enters F-100 where suspended solids such as seaweed and sand are removed and rejected in S200. Seawater exits F-100 in S300 and enters MT-100 where it is mixed with recycled alkaline stream S1100 to stimulate precipitation of $Mg(OH)_2$ based on Equation 12. The enthalpy of formation of $Mg(OH)_2$ is -925 kJ/mol. Solid $Mg(OH)_2$ and water exit MT-100 in S400 and enter rotary drum filter F-200 where solids are removed and rejected in S500. The demineralised water exits in S600 and is split into S700 and S800: S700 proceeds to the first electrolyser, ME-100, and S800 is sent to neutralisation tank MT-200 to control the pH of S1900 which is discharged back to the sea.

$$Mg^{2+}(aq) + 2OH^{-}(aq) \rightarrow Mg(OH)_2(s) \quad (12)$$

In ME-100, the demineralised SW is split into an alkaline cathode effluent, S900, and an acidic anode effluent, S1200, both leaving ME-100 at atmospheric pressure and 50°C. The reaction occurring in ME-100 is given in Equation 13 and the enthalpy change associated with this reaction is 95.9 kJ/mol. The pH of streams S900 and S1200 are 13.2 and 0.8, respectively. A portion of the alkaline stream is sent to the second electrolyser ME-200 in S1000 and the remainder of the stream is recycled back to MT-100. Before entering ME-200, S1000 is pressurised in CP-200 to 10 bar from atmospheric pressure. In ME-200, direct alkaline SW electrolysis occurs based on Equation 7 and produces two streams, one with hydrogen gas and alkali (S1600) and another with oxygen gas and alkali (S1300). Both streams leave at 10 bar and 80°C. The hydrogen gas is separated from the alkali in phase separator FD-100 before being compressed in C-200 to 200 bar and stored in storage tank T-200. Oxygen gas is removed from the alkaline solution in FD-200, exits in S1400 and is then compressed to 350 bar in C-100 before being stored in T-100.

$$H_2O(l) \rightarrow OH^{-}(aq) + H^{+}(aq) \quad (13)$$

The alkaline streams exiting both phase separators, S1500 and S1700, are sent to neutralisation tank MT-200 to be neutralised by excess acid. Forsterite, Mg_2SiO_4, enters in S1210 and is mixed with acidic stream S1200 in mixing tank MT-300. This stimulates the precipitation of solid SiO_2 and neutralises the stream based on Equation 14. The overall enthalpy of this reaction is -70.7 kJ/mol. Solid SiO_2 is then removed in F-300 and rejected in stream S1230. The reaction that occurs in MT-300 also restores the concentration of Mg^{2+} ions to that of input stream S100. The acidic fluid leaves F-300 in S1240 and is sent to MT-200 for neutralisation. Post-neutralisation, water leaves MT-200 in S1900 with the same composition as S100.

$$Mg_2SiO_4(aq) + 4H^+(aq) \rightarrow 2Mg^{2+}(aq) + SiO_2(s) + 2H_2O(l) \qquad (14)$$

Finally, S1900 is cooled in HX-200 to a maximum of 8^{o}C before being discharged to the sea in S2000.

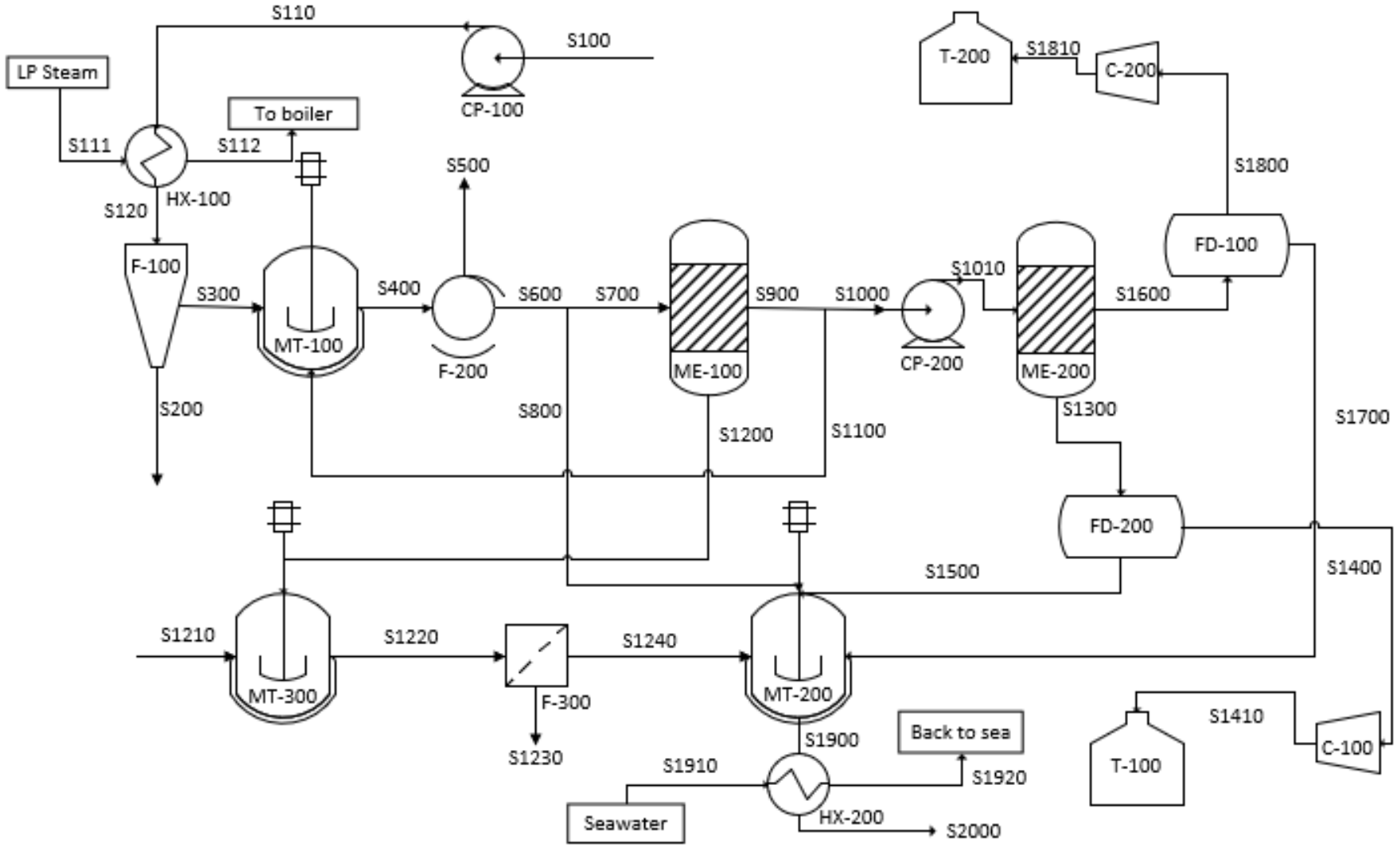

Figure 21 - Process flow diagram for Process 4 (Membrane-less).

3.3 Mass and Energy Balances

Using the process flow diagrams given in Sections 3.2.1 to 3.2.4, mass and energy balances on were carried out based on 1 kg of H_2 being produced per hour. When carrying out the mass and energy balances, the following assumptions were made:

- The process is operating at steady state.
- Each heating/cooling or pressurising/depressurising process operates over one single unit.
- Heating and cooling occurs isobarically.
- Pressurisation and depressurisation of liquids occurs isothermally.
- For alkaline electrolysis, the electrolyser used is the A150 Model Alkaline Electrolyser by Nel and the operating conditions are given in Table 5.
- For PEM electrolysis, the electrolyser used is the M2000 Model PEM Electrolyser by Nel and the operating conditions are given in Table 5.
- For the membrane-less electrolyser process, the electrolyser used is the device designed and patented by Esposito and O'Neil [66].
- Heating and pressurising occurs internally within the electrolysers, except in the case of the membrane-less electrolyser, where the stream is pressurised before entry. The energy consumptions stated in Table 5 are assumed to account for the energy required for heating and pressurising.
- LP steam (1.01 bar, 100^{o}C) is available on site for heating.
- Seawater is used for any cooling and therefore relevant heat exchangers and pipelines are constructed using corrosion resistant materials.
- Seawater feed to each process is pH neutral and 5^{o}C, based on the process plants being located offshore in the North Sea of Scotland.
- The storage pressures for gaseous hydrogen and oxygen are 350 bar and 200 bar, respectively.
- No heat or pressure is lost in pipelines.

Table 5 - Specifications for two types of electrolysers from Nel: the Alkaline A150 Model and the PEM M2000 Model.

Specification	**Nel Electrolyser**	
Type of electrolyser	Alkaline	PEM
Model name	A150	M2000
Operating temperature	70°C	70°C
Power consumption	3.8 - 4.4 kWh/m^3H_2	4.5 kWh/m^3H_2
Output pressure	1 - 200 barg	30 barg
Product purity	99.9% H_2, 99.5% O_2	99.9995%
O_2 in H_2	2 ppm	1 ppm
H_2 in O_2	2 ppm	5 ppm
Water consumption[1]	1.1 kgH_2O/m^3H_2	1.4 kgH_2O/m^3H_2

The energy of each stream, Q, was calculated using Equation 15:

$$Q = m'C_p(T - T_{ref}) \tag{15}$$

Where Q = energy of stream (kW), m' = mass flowrate (kg/s), C_p = heat capacity of stream (kJ/kg.K), T = temperature of stream (K) and T_{ref} = reference temperature (273.15 K). In instances when two streams are mixed, the temperature of the mixed stream was calculated based on Equation 16.

$$T_{1+2} = \frac{(m'_1 C_{P,1} T_1 + m'_2 C_{P,2} T_2)}{(m'_1 C_{P,1} + m'_2 C_{P,2})} \tag{16}$$

The specific heat capacity of each stream, C_p, was found based on a weighted average of the stream apart from in the case of SW or brine, where an online calculator was used to find the heat capacity based on salinity [67].

The area required for heat transfer in heat exchangers is calculated using Equation 17:

$$A = \frac{Q}{U\Delta T_{LM}} \tag{17}$$

Where A = heat transfer area (m^2), U = overall heat transfer coefficient (W/m^2.K) and ΔT_{LM} = log mean temperature difference, which is calculated using Equation 18:

[1] Water consumption was not provided for these models and so was calculated based on an average water consumption of other alkaline/PEM electrolysers.

$$\Delta T_{LM} = \frac{\Delta T_1 - \Delta T_2}{ln\left(\frac{\Delta T_1}{\Delta T_2}\right)} \quad (18)$$

Where ΔT_1 = hot stream temperature in minus cold stream temperature out and ΔT_2 = hot stream temperature out minus cold stream temperature in. The values used for U for water-to-water and steam-to-water heat exchange were 370 W/m^2.K and 1050 W/m^2.K respectively based on mild steel being used as the transmission surface material [68].

The thermal input required by each unit can be calculated based on the law of conservation of energy using Equation 19.

$$Accumulation = In - Out + Generation - Consumption \quad (19)$$

This can be rewritten as shown in Equation 20:

$$\frac{dQ}{dt} = Q_{in} - Q_{out} + Q_R \quad (20)$$

Where $\frac{dQ}{dt}$ is the accumulation of energy over time (kJ/s or kW), Q_{in} is the collective energy of streams entering a unit (kW), Q_{in} is the collective energy of streams exiting a unit (kW) and Q_R is the energy consumed or generated by any reactions taking place (kW) in the unit. If the reaction is endothermic, it will consume heat and Q_R will be positive and if it's exothermic, it will generate heat Q_R will be negative. The processes are all operating at steady state, meaning that in each individual unit the energy within the unit should be constant, i.e. $\frac{dQ}{dt}$ should be equal to zero. If it is found using the energy balance that $Q_{in} - Q_{out} + Q_R$ is not equal to zero, then the resulting value from this equation is the amount of thermal input that is required to the unit. Negative values correspond to cooling and positive values correspond to heating.

3.3.1 Process 1 (Alkaline) Mass and Energy Balance

As well as the assumptions stated in Section 3.2, the following assumptions were made when constructing the mass and energy balances of this process:

- Rejection of ions present in seawater from F-100 occurs based on the values in Table 6. For ions not included in this table, it was assumed they are 100% removed due to the negligible concentrations that are present (Table 4).
- The operating temperature and trans-membrane pressure of F-100 are 25^{o}C and 14 bar respectively, based on [64].

- Water recovery in F-100 is 10% based on [13].
- The concentration of NaOH in T-100 is 40 wt% and the temperature in T-100 is 25°C based on the experiments carried out by Amikam et al [13].
- The solubility of NaCl in T-100 is 90 g/kg H_2O based on Figure 17.
- T-100 is sized so that it can hold 1 kg of water; therefore, the mass of precipitated NaCl is the mass of NaCl in S300 minus 90 g.
- Any dissolved NaCl does not precipitate anywhere other than T-100.
- The oxygen and hydrogen leaving AE-100 in S700 and S800 are both dry and the only impurities are O_2 in H_2 and H_2 in O_2.

Table 6 - Ion rejection rate for various ions during nanofiltration process.

Ion	Rejection rate (%)
Cl^-	28.4
Na^+	4.3
Ca^{2+}	100
Mg^{2+}	100
K^+	32.7
HCO_3^-	37.7

The flowrate of heat transfer fluid into each heat exchanger was found so that this could aid in assessing the feasibility of the processes. The required flowrate of steam through HX-100 was found by first using the energy balance to find the heat input required between S110 and S120. The mass flowrate could then be found using Equation 21:

$$m'_{S130} = \frac{Q_{S110-S120}}{C_{P,S130} \times (T_{S130} - T_{S140})} \quad (21)$$

The specific heat capacity, C_P, of LP steam was taken to be 4.18 kJ/kg.K and the outlet temperature was set to 26°C. This temperature was selected to create the maximum possible temperature difference in the steam so that the flowrate required would be minimised. In HX-300, the temperature difference was fixed at 3°C as this is the maximum temperature difference that seawater can be discharged to the sea at [69]. The flowrates of S620 and S630 were then found using Equation 21.

To find the mass flows of oxygen and hydrogen leaving the electrolyser (S700 and S800 leaving AE-100) the reaction conversion was calculated. The water consumption value from Table 5 was used to find the reaction conversion in the electrolyser, which is defined as the

fraction of water which passes through the electrolyser which is reacted. To produce 1 m^3 of H_2, 1.1 kg of H_2O is required. Using Equation 22, this can be converted to a mass of H_2:

$$m_{H2} = \rho_{H2} V_{H2} \tag{22}$$

Where m = mass (kg), ρ = density (kg/m^3) and V = volume (m^3). Based on an operating temperature of 70°C and density of 0.0706 kg/m^3 at this temperature, the mass of H_2 produced from 1.1 kg of water is found:

$$m = 0.0706\, kg/m^3 \times 1\, m^3$$

$$= 0.0706\, kg$$

As shown previously in Equation 22, during electrolysis, one mole of water reacts to produce one mole of H_2 and 0.5 moles of O_2. Therefore, assuming 100% conversion and knowing that the molecular weights of water, hydrogen and oxygen are 18.02 g/mol, 2.02 g/mol and 31.99 g/mol respectively:

$$18.02\, g\, H_2O \rightarrow 2.02\, g\, H_2 + 15.995\, g\, O_2 \tag{23}$$

Based on this, the theoretical mass of reactants from 1.1 kg of water can be found:

$$1.100\, kg\, H_2O \rightarrow 0.123\, kg\, H_2 + 0.976\, kg\, O_2 \tag{24}$$

The reaction conversion, ε, is then found by dividing the actual mass of hydrogen produced by the theoretical mass, as shown in Equation 25.

$$\varepsilon = \frac{Actual\ mass\ (kgH_2)}{Theoretical\ mass\ (kgH_2)} \tag{25}$$

$$= \frac{0.0706}{0.1230}$$

$$= 0.574$$

Therefore, for every 1 mol of water that passes through the electrolyser, 0.574 mol of H_2 will be produced.

The heat produced by the exothermic reactions occurring in T-100 and AE-100 was found using Equation 26.

$$Q_R = n' \Delta h_R \tag{26}$$

Where Q_R = heat produced by reaction (kW), n' = molar flowrate of reactant (mol/s) and Δh_R = enthalpy of reaction (kJ/mol). For the precipitation reaction given in Equation 11, Δh_R = -411.1 kJ/mol. For the electrolysis reaction occurring in AE-100 which is given in Equation 7, Δh_R = -285.8 kJ/mol.

The impurities in the streams leaving the electrolyser are given in parts per million (ppm) on a volumetric basis. Therefore, to find the composition of S700 and S800, the mass flows were converted to volumetric flows using the densities of the product gases at 70°C (ρ_{H2} at 70°C = 0.0706 kg/m^3 and ρ_{O2} = 1.121 kg/m^3).

The temperature of S710 and S810 were found when calculating compressor work in Section 3.4 using Equation 30 and 31.

3.3.2 Process 2 (PEM 1) Mass and Energy Balance

As well as the assumptions stated in Section 3.2, the following assumptions were made when constructing the mass and energy balance for this process:

- The air entering humidifier H-100 is at 80% relative humidity, which is the global average air humidity directly above sea [40].
- The composition of S120 is as given in Table 7.
- The volumetric flowrate of nitrogen entering in S430 is half of that of the air entering in S300 [40].
- The PSA unit produces hydrogen that is 100% pure; this is based on PSA systems being known to produce hydrogen of a purity up to 99.999% [70].
- The separation efficiency of FD-100 is 100%, which is known to be achievable [71].
- The PSA unit operates isothermally.
- Nitrogen and hydrogen gas leaving PEM-100 in S600 are dry (RH0) and the only impurity is oxygen.
- Heating occurs internally within the humidifier H-100.
- H-100 operates at 80°C and atmospheric pressure [65].

Table 7 - Composition of dry air entering process in S120 [72].

Component	Mole Fraction	Mass (g/mol of air)
O_2	20.95%	6.70
N_2	78.08%	21.87
CO_2	0.04%	0.02
Ar	0.93%	0.37
	Total	28.97

The flowrate of feed seawater (S100) is determined by the flowrate of water being recycled back from the electrolyser in S510 so that the salinity of S210 is equal to S100. The mass of water in S300 is based on the moisture content of air at RH100 and 80ºC (551.04 g H_2O per kg of dry air), which was found using a psychrometric chart. In S120, which is at RH80 and 5ºC, the water content is 4.33 g H_2O/kg dry air.

The reaction conversion was calculated as described in Section 3.2.0; water consumption for the PEM electrolyser was assumed to be 1.4 kg H_2O/m^3 H_2 and the conversion was found to be 0.407. Therefore, for every 1 mol of H_2O that passes through the electrolyser, 0.407 mol of H_2 is produced. Impurities in S700 and S800 were calculated on a volumetric basis using the same densities as stated in Section 3.2.0.

The only chemical reaction occurring in Process 2 is the electrolysis reaction which takes place in PEM-100 based on Equation 10. The heat of this reaction was calculated using Equation 26 and the value for enthalpy of formation of water as stated in Section 3.3.1.

3.3.3 Process 3 (PEM 2) Mass and Energy Balance

As well as the assumptions stated in Section 3.2, the following assumptions were made when constructing the mass and energy balances for this process:

- The HDH unit is 100% efficient in saturating/drying the air stream passing through H-100 and DH-100.
- The operating conditions of the HDH unit are as given by Belessiotis et al in [65]: 1.01 bar and 80ºC.
- Heating occurs internally within the HDH unit.
- The composition of dry air (S400) is as stated in Table 7.
- The separation efficiency of vapour-liquid separator FD-100 is 100%.
- Hydrogen leaving PEM-100 in S700 is dry and the only impurity is oxygen (1 ppm v/v).

- The mass flowrates of S930 and S940 are set so that S1000 has the same salinity and composition as S100.

The flowrate of cooling water (seawater) that flows through HX-100 was calculated based on Equation 19. The temperature difference was set to 3K to ensure that discharged water was at an acceptable temperature. The same specifications were used for the PEM electrolyser as were used in Process 2 (PEM 1) and so the reaction conversion was the same as given in Section 3.2.1 (0.407).

The heat of the water electrolysis reaction occurring in PEM-100 was calculated in the same way as described in Section 3.3.1.

Impurities in S700 and S800 were calculated on a volumetric basis using the same densities as stated in Section 3.2.0. The water content of S300 was found to be 551.04 g H_2O/kg dry air using a psychrometric chart (RH100 and 80^oC).

3.3.4 Process 4 (Membrane-less) Mass and Energy Balance

As well as the assumptions stated in Section 3.2, the following assumptions were made when constructing the mass and energy balances for this process:

- The mass flowrate of S200 will vary so it is not included in the mass balance. However, it is assumed that 100% of suspended solids are removed in F-100.
- Due to its low solubility in water (solubility product, K_{sp}, is 5.61 x 10^{-12} [73]), the amount of $Mg(OH)_2$ present in the stream post precipitation in MT-100 and filtration in F-200 is negligible.
- Filtration units F-200 and F-300 are both 100% effective at removing the precipitated solids.
- The conversion of the reaction occurring in MT-300 given in Equation 14 is 100%.
- The concentration of Mg^{2+} ions post F-200 is negligible.
- Phase separators FD-100 and FD-200 operate at 100% separation efficiency.
- No dissolved ions other than Mg^{2+} are involved in chemical or electrochemical reactions.
- Cl^- is never oxidised in either ME-100 or ME-200 based on the electrocatalysts that are used.
- Mass flowrate of water into ME-200 is controlled so that the salinity of S1000 is limited to 5%.

- The reactions occurring in MT-100, MT-200 and MT-300 are not temperature dependent and so the operating temperatures are not fixed.

The mass balance was partially constructed based on known pH levels of the streams. For example, in alkaline stream S900, the pH was known to be 13.2. Therefore, the concentration of OH^- ions in that stream was calculated based on Equation 27.

$$-\log[OH^-] = 14 - pH \tag{27}$$

$$[OH^-] = 10^{-0.8}$$
$$= 0.158\ mol/L$$

The outlet temperatures of MT-100, MT-200 and MT-300 were calculated by varying the outlet temperature and therefore the heat of the outlet stream, Q_{out}, until the steady state energy change was equal to zero based on Equation 20.

The reaction conversion in electrolysers ME-100 and ME-200 was based on values for mass flowrates of product streams provided by sHYp.

The heat of the reactions given in Equations 12, 13 and 14 were found as described in Section 3.4.1 using Equation 26. The enthalpy of reaction for Equations 12, 13 and 14 was -925 kJ/mol, 95.9 kJ/mol and -70.7 kJ/mol, respectively.

3.4 Electrical Power Consumption

The electrical power consumed by equipment in all processes was calculated to find the overall energy demand of the process. It was assumed that the only power-consuming units were pumps, compressors and electrolysers. The power consumption of centrifugal pumps was calculated based on Equation 28.

$$P_e = \frac{\Delta P V'}{\eta_{CP}} \times 100 \tag{28}$$

Where P_e = electrical power (W), ΔP = change in pressure (Pa), V' = volumetric flowrate (m^3/s) and η_{CP} = pump efficiency, which was assumed to be 90% for all pumps [74].

The power consumed in gas compressors was calculated based on Equation 29.

$$P_e = m' C_P (T_{out} - T_{in}) \tag{29}$$

Where m' = mass flowrate (kg/s), T_{out} = temperature of compressor outlet stream (K) and T_{in} = temperature of compressor inlet stream (K). The isentropic temperature of the outlet stream, T_{out}' was calculated using Equation 30.

$$T'_{out} = T_{in} \times \left(\frac{P_{out}}{P_{in}}\right)^{\frac{\gamma-1}{\gamma}} \quad (30)$$

Where P_{out} = pressure of compressor outlet stream (bar), P_{in} = pressure of compressor inlet stream (bar) and γ is specific heat ratio, i.e. C_P/C_V. The values for γ are given in Table 8. The real temperature of the outlet stream was then calculated using Equation 31.

$$T_{out} = \frac{T'_{out} - T_{in}}{\eta_C} + T_{in} \quad (31)$$

Where η_C = isentropic efficiency of compressor, which was taken to be 85% for all compressors [75].

Table 8 - Values for specific heat capacity at constant pressure, specific heat capacity at constant volume and specific heat ratio for oxygen and hydrogen gas.

Gas	C_P (kJ/kg.K)	C_V (kJ/kg.K)	γ
Oxygen	0.919	0.659	1.395
Hydrogen	14.320	10.160	1.409

The power consumption of the alkaline and PEM electrolysers was given in Table 5 based on the volumetric flowrate of hydrogen gas produced. The energy consumption of membrane-less electrolysers in Process 4, ME-100 and ME-200, were provided by sHYp as 0.5 kWh/kgH_2 and 59 kWh/kgH_2, respectively.

3.4.1 Process 1 (Alkaline) Power Consumption

Power-consuming equipment in Process 1 included centrifugal pump CP-100, alkaline electrolyser AE-100 and two compressors, C-100 and C-200.

The volumetric flowrate through the pump was found by converting mass flowrate from kg/h to kg/s and using Equation 22. The electrical power consumption was then found using Equation 32.

$$P_{e,CP-100} = \frac{(P_{S110} - P_{S100}) \times V'_{S100}}{\eta_{CP-100}} \times 100 \quad (32)$$

$$P_{e,CP-100} = \frac{(1{,}501{,}325 - 101{,}325\ Pa) \times 2.5 \times 10^{-5}\ m^3/s}{0.9} \times 100$$

$$= 3.93\ kW$$

The process produces 1 kg H_2 per hour so the electrical consumption of CP-100 can be stated as 3.93 kWh/kgH_2.

The maximum electrical consumption for AE-100 is 4.4 kWh/m^3 H_2 (Table 5). This is the electricity consumption of the electrolyser stack only. Dividing by the density of hydrogen gas at 70°C (0.0706 kg/m^3) converts this value into 62.32 kWh/kg H_2.

The electrical power input to C-100, which compresses oxygen, was found by first finding the isentropic temperature of S710 using Equation 33.

$$T'_{S710} = T_{S700} \times \left(\frac{P_{S710}}{P_{S700}}\right)^{\frac{\gamma-1}{\gamma}} \quad (33)$$

$$= 343.15\ K \times \left(\frac{200\ bar}{30\ bar}\right)^{\frac{1.395-1}{1.395}}$$

$$= 687.61\ K$$

The real temperature of S710 was then calculated using Equation 34.

$$T_{S710} = \frac{T'_{S710} - T_{S700}}{\eta_{C-100}} + T_{S700} \quad (34)$$

$$= \frac{687.61 - 343.15}{0.85} + 343.15$$

$$= 748.40\ K$$

This value could then be used to calculate to electrical power consumed by C-100 during this compression process using Equation 35.

$$P_{e,C-100} = m'_{S700} C_{P,S700} (T_{S710} - T_{S700}) \quad (35)$$

$$= \left(\frac{7.93\frac{kg}{h}}{3600\frac{s}{h}}\right) \times 0.919\frac{kJ}{kg}.K \times (748.40 - 343.15)$$

$$= 0.82\ kWh/kgH_2$$

The power consumed by the hydrogen compression process in C-200 was found using the same method with temperature and pressure values corresponding to S800 and S810. The total electrical power consumption of the process was found by summing the values for all the individual components.

3.4.2 Process 2 (PEM 1) Power Consumption

The power-consuming components in Process 2 were identified as centrifugal pump CP-100, PEM electrolyser PEM-100 and hydrogen compressor C-200. The electrical power consumed by these units was calculated using the same methods as described in Section 3.4.1.

3.4.3 Process 3 (PEM 2) Power Consumption

Four units which consume electrical power were identified in Process 3: centrifugal pump CP-100, PEM electrolyser PEM-100 and two compressors, C-100 and C-200. Again, the electrical power consumed per kg of H_2 was calculated using methods described in Section 3.4.1.

3.4.4 Process 4 (Membrane-less) Power Consumption

Centrifugal pumps CP-100 and CP-200, membrane-less electrolysers ME-100 and ME-200 and compressors C-100 and C-200 were all identified as being electricity consuming units. The electrical power consumed was calculated using methods described in Section 3.4.1 with the electrolyser consumption values provided by sHYp.

3.5 Comparison of Membrane-less Technologies

For each of the devices discussed in Section 2.2, the following parameters were obtained:

- Maximum current density
- Onset potential
- Flowrate or flow velocity
- Channel diameter
- Product cross-over
- Electrode separation distance
- Cell voltage at a current density of 100 mA/cm^2

These values were then used to find the voltage efficiency and the Gibbs' free energy efficiency of each membrane-less device. The voltage efficiency was measured using the cell voltage at

a current density of 100 mA/cm^2 for each device to ensure consistency. The voltage efficiency, η_V, was calculated using Equation 36, with the standard cell potential of water electrolysis, E^o_{cell}, being 1.229 V.

$$\eta_V = \frac{E^o_{cell}}{E_{cell}(@\ 100\, mA/cm^2)} \tag{36}$$

The cell voltages of the electrolyser devices were found from J-V graphs (Appendix 2) given in the relevant research papers unless the voltage at 100 mA/cm^2 was stated in the text. The efficiency based on the higher heating value (HHV) of hydrogen, η_{HHV}, was found using Equation 37, where the HHV value of H_2 was 285.8 kJ/mol and ΔG^o_f is the Gibbs' free energy of the formation of water (237.2 kJ/mol).

$$\eta_{HHV} = \frac{\eta_V \times HHV_{H2}}{\Delta G^o_{f(H2O)}} \tag{37}$$

As well as efficiency, the Reynolds' number of the flow in the main channel of each electrolyser cell was calculated using Equation 38.

$$Re = \frac{du\rho}{\mu} \tag{38}$$

Where d = diameter of the channel (m), u = velocity of flow in the channel (m/s), ρ = density of the fluid in the channel (kg/m^3) and μ = dynamic viscosity of the fluid in the channel (kg/m.s). This value was calculated so that it could be determined whether there was any correlation between Reynolds' number within the fluid channel and efficiency of the electrolyser device, based on hypotheses made by Hashemi et al regarding the relationship between flow regime and performance of electrolyser cells discussed in Section 2.2 [52].

The Evolve™ C-37 electrolyser was not included in this analysis due to the lack of available information on this device.

4.0 Results and Discussion

4.1 Mass and Energy Balance Results

From the mass and energy balances for each process (given in Appendix 1), it was possible to determine the overall throughput of seawater in the electrolysis system. In this context, this includes seawater used as a feedstock and for cooling in heat exchangers but does not include seawater that may be used for cooling in any equipment such as electrolysers. The results are

given in Table 9. For comparison, producing hydrogen using water electrolysis has been shown in previous studies to consume anywhere between 8,820 and 223,390 kg of water per kg of hydrogen produced [76].

Processes 2 and 4 (PEM 1 and Membrane-less) used significantly more water than the other processes (311,751 and 376,305 kg SW/kg H_2 respectively). For Process 2, a relatively high flowrate of seawater was required as feed so that the unreacted water from the electrolysis stage would be sufficient to return this stream to its original salinity. In Process 4, a high throughput of feed water is required because a large proportion of the water that passes through the first electrolyser (~98%) is recycled back to the mixing tank to stimulate $Mg(OH)_2$ precipitation. An alternative process design which incorporates a membrane-less electrolyser but does not produce $Mg(OH)_2$ as a by-product could potentially have a reduced seawater throughput in comparison to the process analysed here, but it is unknown what impact the harmful Mg^{2+} ions would have on the performance of the membrane-less electrolyser.

Table 9 – Mass of seawater used in each process for feedstock and for cooling.

	Water Throughput (kgSW/kgH2O)		
Process	**Feed**	**Cooling**	**Total**
1 (Alkaline)	91	610	701
2 (PEM 1)	12,371	299,379	311,751
3 (PEM 2)	34	781	814
4 (Membrane-less)	22,613	353,891	376,305

As a knock-on effect of large feed streams, the flowrate of seawater used to cool streams in Processes 2 and 4 was also relatively high, leading to a higher overall throughput of water. Processes 1 (Alkaline) and 3 (PEM 2) used similar flowrates of water (701 and 814 kg SW/kg H_2, respectively). It should be noted that a significant portion (up to 96%) of the water throughput for every process was used for cooling, due to the maximum allowable temperature difference between the inlet and outlet streams being 3^{o}C. This suggests that perhaps for these systems, a different cooling method should be adopted rather than using seawater; a passive approach in which discharged water was stored in tanks and allowed to cool naturally would use less energy and therefore improve the efficiency of the systems.

The mass flowrates of certain streams were optimised so that any water discharged to the sea was rejected at its initial salinity. Therefore, an increased seawater throughput should not increase the danger of harming sea life or destabilising the local oceanic environment. Furthermore, as these processes are intended for offshore hydrogen production, seawater

availability will not be an issue. However, there are still negative impacts associated with a large water throughput. Based on Equation 28, an increase in seawater throughput of the system correlates to a greater electrical power requirement of centrifugal pumps. This will therefore decrease the overall energy efficiency of the system based on 1 kg of H_2 being produced. Furthermore, the larger the flowrate of fluid through any equipment, the larger the equipment will have to be. This applies to pumps, heat exchangers, pipelines and any processing units involved in the system. For most components of these systems, there is a direct correlation between size and cost of equipment. Therefore, an increased liquid flowrate results in a greater overall capital cost of the system.

In addition to this, due to its high salinity, seawater is extremely corrosive. Processing equipment used in marine environments is subject to several different types of corrosion such as uniform corrosion, galvanic corrosion and biofouling [77]. The higher the flowrate of seawater, the more susceptible pipelines and equipment will be to corrosion. Corrosion-resistant coatings can be used to minimise the issue, but there will still be increased maintenance required so ensure corrosion is kept to a minimum [78]. Increased maintenance will result in an increase in annual operation and maintenance (O&M) costs of the system.

Table 10 - Thermal input required for each process for both heating and cooling.

	Thermal Input (kWh/kgH2)	
Process	**Heating**	**Cooling**
1 (Alkaline)	2	-43
2 (PEM 1)	1031	-1037
3 (PEM 2)	3	-42
4 (Membrane-less)	377	-1271

Another parameter of the processes that was considered was the thermal input required for both heating and cooling. The results are given in Table 10. All of the processes required more energy for cooling than they did for heating, due to the exothermic reactions taking place in the electrolysers. In Process 4 (Membrane-less), an endothermic reaction occurs in the first electrolyser. However, because the temperature of the entering stream was raised by the exothermic precipitation reaction, this electrolyser still requires cooling to maintain the operating temperature of 50^{o}C. Process 2 (PEM 1) required the greatest level of thermal input (2068 kWh/kgH_2 in total), due to the high volume of fluid that is heated in humidifier H-100 and then cooled in HX-100 before being discharged to the sea. Process 4 requires a relatively high cooling input (1037 kWh/kg H_2); however, as previously mentioned, a passive system

could reduce this. Processes 1 and 3 required similar thermal inputs for both heating and cooling (45 kWh/kg H_2 total for each process).

An increase in thermal input will increase the total energy input required to produce 1 kg of H_2 and therefore reduce the energy efficiency of the whole system. Furthermore, increased heating and cooling requirements will increase the volume of fluid that is pumped through the system to transfer heat, which will further increase the total energy input to the system.

The total thermal input to each process can be reduced through better utilisation of any waste heat that is produced. This could be achieved by performing a pinch analysis, in which units or streams that need to gain heat are matched with those that need to lose heat. For example, in Process 2 (PEM 1), the heating input almost exactly matches the cooling input (1031 versus 1037 kWh/kgH_2), meaning there is a lot of potential for stream matching; the excess heat in streams S500 and S600 leaving the electrolyser could be used to heat the fluid in humidifier H-100 instead of using steam which will require a boiler on site. Additionally, excess heat produced in any compression stages in the processes could be used to heat other streams. For example, in Process 1 (Alkaline), waste heat from compressors C-100 or C-200 which are used to compress hydrogen and oxygen could be used to heat stream S110 in heat exchanger HX-100.

4.2 Electrical Power Consumption Results

Using the methods stated in Section 3.4, the electrical power consumed by each pump, compressor and electrolyser in each process was calculated. The results are given in Table 11. In each process apart from Process 4 (Membrane-less), the electrolyser was the biggest power-consuming component. The PEM electrolyser consumed slightly more power than the other two types of electrolysers. As a stand-alone unit, the membrane-less electrolyser consumed the least electrical power of all the electrolysers (0.5 kWh/kg H_2 in ME-100 and 59.0 kWh/kg H_2 in ME-200).

Table 11 - Electrical power consumed in each process by pumps, compressors and electrolysers.

	Electrical Power Consumption (kWh/kgH2)			
Process	**Pumps**	**Compressors**	**Electrolysers**	**Total**
1 (Alkaline)	3.83	2.25	62.32	68.40
2 (PEM 1)	36.67	1.67	63.74	102.09
3 (PEM 2)	0.10	4.50	63.74	68.34
4 (Membrane-less)	75.01	7.24	59.50	141.75

Process 4 (Membrane-less) was found to consume the most electrical power per kg of H_2 out of all the processes. However, it is important to note that this process was the only one in which it was necessary to raise the pressure of the stream entering the electrolyser to its operating pressure. This assumption was made based on the flow diagram provided by sHYp. For the PEM and alkaline electrolysers, it was assumed based on the specification sheets that pressurisation occurred internally within the electrolyser and was therefore already accounted for in the total electrical power consumption value provided by the manufacturers. If this assumption had not been made, the electrical power consumption attributed to pumps in the other processes would be greater. With this being said, most of the pumping power in Process 4 (Membrane-less) came from the feed pump, CP-100 (67.04 kWh/kgH_2), and not the electrolyser pump, CP-200 (7.97 kWh/kg H_2), so the electrical consumption was still high in comparison to the other processes.

Process 2 (PEM 1) also required a relatively high level of pumping power (37.68 kWh/kgH_2). This is due to the high volumetric flowrate passing through the pump, CP-100. As stated previously, increased power consumption not only reduces the overall energy efficiency of the process but it also drives up the costs associated with producing hydrogen.

The electrical power consumption discussed in this section is only meant to provide a comparison relative to the other processes and does not cover all of the power consuming elements. For example, some of the filtration units such as F-100 in Process 1 (Alkaline) will also consume electrical power. If there had not been limitations with the software that was available to use to simulate these processes (discussed in Section 2.4), a more detailed analysis could have been given. Therefore, the values given in this section should not be taken as absolute.

4.3 Overall Comparison of Processes

Based on the total power consumption (electrical and thermal) of each process and the HHV of hydrogen gas (39.4 kWh/kg), the overall energy efficiency of each process was calculated. The results are given in Table 12. These efficiencies are similar to those found by Demir and Dincer and Delpisheh et al when analysing processes for producing hydrogen from seawater [35] [36]. Processes 1 and 3 had similar efficiencies and were the most efficient overall, which was expected based on both their thermal inputs and electricity consumptions discussed in Sections 4.1 and 4.2. Processes 2 and 4 also show similar overall efficiencies (~2%), with the membrane-less process being marginally more efficient. However, it is emphasised that this is

based on only one particular set-up involving a membrane-less device; the same electrolyser used within a different process design may yield better results than the other processes. The membrane-less electrolyser on its own is more efficient than either the PEM or the alkaline electrolyser.

Table 12 - Total (electrical and thermal) power consumption of each process based on production of 1 kg of hydrogen gas and the overall energy efficiency of the process based on this value and the HHV of hydrogen.

Process	Total power consumption (kWh/kgH_2)	Efficiency (based on HHV)
1 (Alkaline)	113.3	34.8%
2 (PEM 1)	2170.0	1.8%
3 (PEM 2)	113.6	34.7%
4 (Membrane-less)	1790.0	2.2%

As well as being the least efficient and having one of the highest seawater throughputs, Process 2 (PEM 1) was also found to be practically unfeasible for various other reasons. Firstly, it is the only process in which there is only one product formed (Table 13). This means that there is less product to sell, which leads to less profits and a longer return on any capital investment which was made. The process also required nitrogen gas as a feedstock whereas most of the other processes only used seawater which would further drive up the costs of this process. Furthermore, because the hydrogen gas exits the electrolyser mixed with another gas as opposed to the other processes in which hydrogen is mixed with a liquid, separation of the product gas becomes more complex and costly. The PSA unit used for gas separation requires an adsorbent such as a molecular sieve which will need replaced periodically, increasing the overall costs of the process [79].

Table 13 - Mass flowrates of hydrogen gas and any other valuable by-products from all 4 processes being evaluated.

	Product Flowrates (kg/h)			
Process	**H_2**	**O_2**	**$Mg(OH)_2$**	**SiO_2**
1 (Alkaline)	1.0	7.9	-	-
2 (PEM 1)	1.0	-	-	-
3 (PEM 2)	1.0	7.9	-	-
4 (Membrane-less)	1.0	8.1	64.7	33.6

The area required for any heat exchangers involved in the processes was estimated using Equation 17 to help assess the feasibility. Heat exchanger HX-200 in Process 4 (Membrane-less) was found to be the largest at 199.6 m^2, which is not viable due to the excessively large area that would be needed to accommodate this. In Process 2 (PEM 1), the heat transfer area required for HX-100 was also unreasonably large at 124.1 m^2. These could be reduced in size by performing the heat transfer over several stages instead of one unit or by using an alternative heat transfer fluid rather than seawater so that the temperature difference doesn't need to be kept to 3°C. Any other heat exchangers involved in the processes were found to require a heat transfer area less than 10 m^2 and so were deemed viable.

In all of the compression stages present in the processes, hydrogen and oxygen are compressed from either atmospheric pressure or 30 bar to their respective storage pressures in a single step. In every case, this exceeds the maximum pressure ratio that is possible in a compressor [75]. Therefore, these compression processes would not be feasible in a single stage and would have to occur across multiple stages which would increase the total power consumption.

Although Process 4 (Membrane-less) was the most complex of the systems and had the most components (Figures 19 to 22), it also produced the greatest mass of valuable by-products as seen in Table 13. The market for $Mg(OH)_2$ has been driven up recently by the desire to find an environmentally friendly flame-retardant additive [80]. There is also a growing demand for SiO_2 in the construction industry, making these both profitable by-products [81]. This, combined with the simple membrane-less design of the electrolyser, increases the economic feasibility of this process and will reduce the overall price of producing hydrogen in comparison to the other processes. Furthermore, the use of PEM or alkaline electrolysers with more components than a membrane-less electrolyser means that components will need replaced more regularly and will be more subject to degradation, which will increase the annual O&M costs.

As previously mentioned in Sections 2.1 and 2.2, most of these processes are currently only in the research and development stage and have not been tested using real seawater. During research that Process 1 (Alkaline) was based on, the system was only tested using an NaCl solution as the electrolyte. Process 3 (PEM 2) was based on a study involving only simulated experiments; however, HDH has been proven to be a feasible option for seawater desalination [82]. Process 2 (PEM 1), in which seawater vapour was electrolysed, was in fact tested using real seawater and a commercially available PEM electrolyser, making it more feasible for real-

life, scaled up applications. In any research that Process 4 (Membrane-less) was based on, the only seawater tested was 'synthetic seawater', i.e. 0.6M NaCl solution.

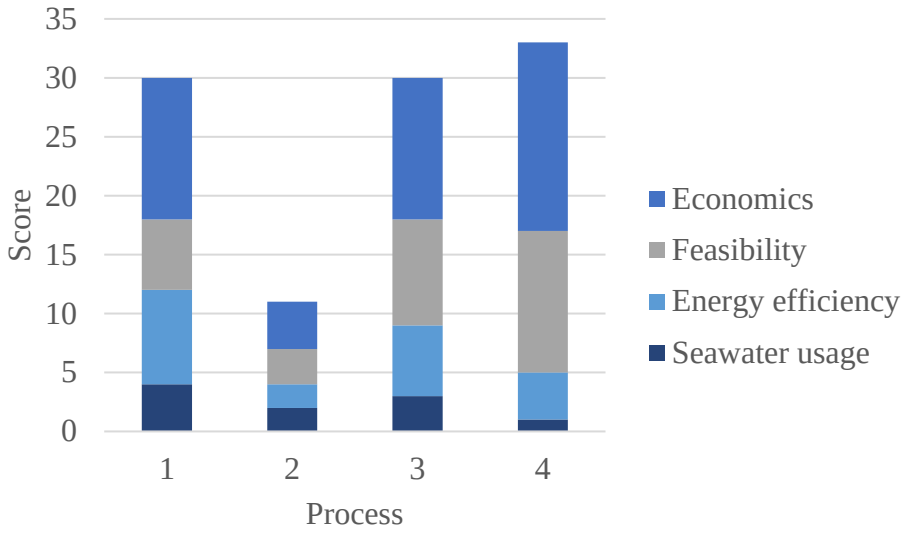

Figure 22 - Bar chart showing how each process scored relative to one another in the categories of economics, feasibility, energy efficiency and seawater usage.

A weighted decision matrix was created in which the four processes were evaluated based on economics, feasibility, efficiency and seawater usage. These factors are listed in order of deemed importance and were weighted accordingly. The resultant scores are displayed in Figure 22. Process 4 (Membrane-less) scored the highest due to its attractive economic benefits, whereas Process 2 (PEM 1) scored the lowest due to having the lowest efficiency, undesirable economics and a high throughput of seawater. Processes 2 and 3 came in closely behind Process 4 and therefore show good promise for being feasible options for producing hydrogen from seawater.

4.4 Comparison of Membrane-less Technologies

Information extracted from relevant research papers regarding performance of each of the identified membrane-less electrolysers is given in Table 14. Higher current densities are desirable as this correlates to the rate of hydrogen production [83]. The device presented by Gillespie et al reached the highest current density of all the devices at around 4000 mA/cm^2. However, this was achieved at a cell voltage of 3.5 V, which results in a voltage efficiency of only 35% and a HHV efficiency of 42%. The second device presented by Hashemi et al (Device No. 7) exhibited the second highest maximum current density of 720 mA/cm^2, which was achieved at a cell voltage of 3.25 V, but in this research the device was configured to produce chlorine gas rather than the more desirable oxygen.

Table 14 - List of membrane-less devices identified along with inventors, electrolyte tested in research, electrolysis products, maximum current density achieved using the device, tested flow velocity, diameter of main channel and product cross-over experienced.

Membrane-less Device No.	Inventors	Electrolyte	Electrolysis Products	Max Current Density (mA/cm^2)	Flow Velocity (m/s)	Channel Diameter (µm)	Product Cross-Over (%)
1	Hashemi et al [42]	1 M H_2SO_4	H_2 and O_2	300	0.449	105	0.4
2	Gillespie et al [45]	30 wt% KOH	H_2 and O_2	~ 4000	0.200	2500	-
3	O'Neil et al [47]	0.5 M H_2SO_4	H_2 and O_2	150	0.132	1.3 cm x 5 cm (rectangular channel)	2.8
4	O'Neil et al [49]	1 M H_2SO_4	H_2 and O_2	105	0.006	1.3 cm x 5 cm (rectangular channel)	-
5	Rarotra et al [50]	Seawater and saline water (0.6 g/L)	H_2 and O_2	-	0.340	500	-
6	Davis et al [51]	0.6 M NaCl	H_2 and O_2	300	N/A	N/A	1
7	Hashemi et al [44]	20 wt% NaCl	H_2 and Cl	706	0.424	1000	-

The total resistance experienced in an electrolyser cell is given in Equation 39:

$$R_{total} = R_{anode} + R_{O_2(g)} + R_{electrolyte} + R_{membrane} + R_{cathode} + R_{H_2(g)} \quad (39)$$

Where R_{anode} is the resistance related to OER, $R_{O2(g)}$ is the resistance associated with void formation on the anode when oxygen gas is formed, $R_{electrolyte}$ is the resistance of the electrolyte solution, $R_{membrane}$ is the resistance of the membrane or diaphragm, $R_{cathode}$ is the resistance related to HER and $R_{H2(g)}$ is the resistance associated with gas formation on the cathode [45]. Removing the membrane of the electrolyser therefore reduces the total resistance experienced and should theoretically allow for higher current densities to be achieved. However, the maximum current density reached by the majority of the devices shown in Table 14 fell short of the current densities that are achieved by commercially available electrolysers (Table 1). This highlights that there is still a lot of further research and development required in this subject area before membrane-less electrolysers are likely to become competitive with alkaline and PEM electrolysers.

Table 15 - Calculated parameters of seven membrane-less electrolysers regarding efficiency and flow regime.

Membrane-less Device No.	Inventors	Cell voltage at ~100 mA/cm^2 (V)	Electrode separation (mm)	Voltage Efficiency	HHV Efficiency	Re Number
1	Hashemi et al	2.50	0.11	49.2%	59.2%	52.2
2	Gillespie et al	1.75	2.5	70.2%	84.6%	0.1
3	O'Neil et al	2.30	13	53.4%	64.4%	891.0
4	O'Neil et al	2.00	13	61.5%	74.0%	45.5
5	Rarotra et al	Unknown	10	-	-	187.1
6	Davis et al	2.50	2.5	49.2%	59.2%	N/A
7	Hashemi et al	2.40	1.0	51.2%	61.7%	269.0

Furthermore, based on Equation 39, it was hypothesised that electrolysers with a smaller electrode separation should be able to reach higher current densities at lower voltages because the resistance associated with the electrolyte solution is reduced. This hypothesis was proven to be true when the angle of separation and therefore distance between the electrodes in an electrolyser device was varied in work by Davis et al [51]. However, on inspection of the values given in Table 15, there does not appear to be any strong link between electrode separation and voltage efficiency. When the electrode separation of each device in Table 15 was plotted against voltage efficiency, the general trend was found to be that efficiency increased with decreasing electrode separation, although this was a very weak correlation; the R^2 value of the trendline was 0.0522. This graph can be found in Appendix 3.

In work by Hashemi et al [52], it was suggested that higher Reynolds' numbers induced by more turbulent flow regimes can have a negative impact on the performance of electrolyser cells due to the higher prevalence and coalescence of gas bubbles. Gas bubbles increase the total electrolysis resistance. This limits the scalability of these devices as increased channel diameter makes it increasingly difficult to maintain the flow as laminar, based on Equation 38. For this reason, the relationship between Reynolds' number and efficiency was investigated. The values for these two parameters for each of the devices are given in Table 15. Based on this, there does not appear to be any strong correlation between Reynolds' number and cell efficiency. When these values were plotted against each other in a graph

with a line of best fit, another weak relationship was found in which HHV efficiency increases with decreasing Reynolds' number. This graph can be found in Appendix 3.

Although there was no strong correlation found between these parameters when analysing these seven different membrane-less devices, it is important to note that there are vast differences between all these designs and the pool of data available was limited. Should similar evaluations be carried out on a single device in which flow regime and electrode separation are varied, it is expected that a different conclusion would be reached.

5.0 Conclusions

In conclusion, hydrogen demand is likely to increase in the future with increased integration of renewable energy technologies. Meeting this demand using seawater electrolysis is one of the more sustainable pathways of the options available for producing hydrogen. If this can be achieved using membrane-less electrolysers, costs can potentially be significantly reduced.

The most common methods that appear in literature for producing hydrogen from seawater electrolysis involve some sort of membrane or thermal distillation before being passed into a PEM or alkaline electrolyser. These processes appear to be feasible since most of them incorporate already well-established technologies such as HDH. However, most of the studies involve only computerised simulations and no real-life experimentation, meaning further investigation is required before these processes can be deployed at scale.

It was found that the majority of membrane-less electrolysers currently being researched are microfluidic devices, which face reduced solution resistance due to the very narrow electrode separation distance (less than < 1 mm in some devices) but may encounter difficulties in scalability. Although many of the membrane-less electrolyser devices identified in literature have now been patented, there are still not any that are commercially available or have been tested beyond laboratory-scale experiments.

Of the four processes that were analysed in detail, all showed merit in some areas and inferiority in others. Processes 2 (PEM 1) and 4 (Membrane-less) both used significant volumes of feed seawater to produce hydrogen (between 12,000 and 23,000 kg of SW per kg of H_2 gas). If these processes are planned for offshore use, then seawater availability will not be an issue, but the impact that this large seawater throughput would have on equipment size and energy usage is significant. All four of the processes used more seawater for cooling than as a feedstock and required more cooling than heating due to the exothermic water electrolysis reactions taking place.

Processes 1 (Alkaline) and 3 (PEM 2) used a significantly smaller throughput of seawater and consequently had a greater overall energy efficiency, making them a lot more practically feasible. Process 4 (Membrane-less) had the second lowest overall efficiency (2.2%) but the membrane-less electrolyser on its own was more efficient than the PEM or alkaline electrolysers. All of the processes could see their energy efficiency or seawater throughput improved if there were some adjustments made to the process design.

For hydrogen gas to be competitive in the fuels market, it must be produced in a way which is economically feasible. Process 4 (Membrane-less) appears to be the most economically attractive, due to the simpler design of the electrolyser and the valuable by-products that are produced. Processes 1 to 3 lacked these by-products and use electrolysers that are more complex and more likely to be subject to degradation, which will increase O&M costs. Overall, Process 2 (PEM 1) was considered to be the least practically feasible of all the processes due to its low efficiency, high seawater throughput, lack of economic benefits and complicated separation process.

No solid conclusion could be drawn regarding the relationship between electrode separation distance, flow regime and voltage efficiency in a membrane-less electrolyser due to the small pool of data available. However, it can be concluded that these devices are not yet at the stage of achieving current densities as high as those experienced in commercially available PEM and alkaline electrolysers.

5.1 Future Work

The work completed in this thesis can be expanded in the future by creating more detailed models of more processes. The lack of appropriate software which was available when completing this work had a negative impact of the complexity of the models; for example, it may have been possible to further optimise the processes through stream-matching and therefore improve the efficiency if a software program was used. Furthermore, the total power consumption of all units in the processes, such as filtration units, could have been included. It would also be beneficial to analyse alternative designs of the membrane-less electrolyser process to see how the efficiency and seawater throughput compares when by-products are not produced.

Membrane-less electrolysers for hydrogen production are a relatively new concept and it is expected that more research will be carried out in this area in coming years. Therefore, when more data is available and more devices have been tested using seawater, another study comparing all the available devices should be carried out in which the impact of flow regime and electrode separation distance can be further analysed.

6.0 References

[1] United Nations, “The Paris Agreement,” United Nations, 12 December 2015. [Online]. Available: https://unfccc.int/sites/default/files/english_paris_agreement.pdf. [Accessed 24 June 2021].

[2] V. Masson-Delmotte, P. Zhai, A. Pirani, S. L. Connors, C. Pean, S. Berger, N. Caud, Y. Chen, L. Goldfarb, M. I. Gomis, M. Huang, K. Leitzell, E. Lonnoy, J. B. R. Matthews, T. K. Maycock, T. Waterfield, O. Yelekci, R. Yu and B. Zhou, “Climate Change 2021: The Physical Science Basis. Contribution of Working Group I to the Sixth Assessment Report of the Intergovernmental Panel on Climate Change,” Cambridge University Press, 2021.

[3] International Energy Agency, “Tracking Clean Energy Progress,” [Online]. Available: https://www.iea.org/topics/tracking-clean-energy-progress. [Accessed 24 June 2021].

[4] D. Heiserman, Exploring chemical elements and their compounds, McGraw-Hill, 1991.

[5] Z. Abdin, A. Zafaranloo, A. Rafiee, W. Merida, W. Lipinski and K. Khalilpour, “Hydrogen as an energy vector,” *Renewable and Sustainable Energy Reviews,* vol. 120, p. 109620, 2020.

[6] S. Sharma and S. K. Ghoshal, “Hydrogen the future transportation fuel: From production to applications,” *Renewable and Sustainable Energy Reviews,* vol. 43, pp. 1151-1158, 2015.

[7] A.T. Kearney Energy Transition Institute, “Hydrogen-based energy conversion,” February 2014. [Online]. Available: https://www.energy-transition-institute.com/documents/17779499/17781876/Hydrogen+Based+Energy+Conversion_FactBook.pdf/ab80d85b-faa3-9c7b-b12f-27d8bad0353e?t=1590787502834. [Accessed 30 June 2021].

[8] A. Ursua, L. M. Gandia and P. Sanchis, “Hydrogen Production From Water Electrolysis: Current Status and Future Trends,” *Proceedings of the IEEE,* vol. 100, no. 2, pp. 410-426, 2012.

[9] M. Carmo, D. L. Fritz, J. Mergel and D. Stolten, “A comprehensive review on PEM water electrolysis,” *International Journal of Hydrogen Energy,* vol. 38, no. 12, pp. 4901-4934, 2013.

[10] A. Ophir and A. Gendel, “Adaptation of the Multi-Effect Distillation (MED) process to yield high purity distillate for utilities, refineries and chemical industry,” *Desalination,* vol. 98, pp. 383-390, 1994.

[11] F. Dionigi, T. Reier, Z. Pawolek, M. Gliech and P. Strasser, "Design Criteria, Operating Conditions, and Nickel–Iron Hydroxide Catalyst Materials for Selective Seawater Electrolysis," *ChemSusChem,* vol. 9, no. 9, pp. 962-972, 2016.

[12] S.-H. Hsu, J. Miao, L. Zhang, J. Gao, H. Wang, H. Tao, S.-F. Hung, A. Vasileff, S. Z. Qiao and B. Liu, "An Earth-Abundant Catalyst-Based Seawater Photoelectrolysis System with 17.9% Solar-to-Hydrogen Efficiency," *Advanced Materials* , vol. 30, no. 18, 2018.

[13] G. Amikam, P. Nativ and Y. Gendel, "Chlorine-free alkaline seawater electrolysis for hydrogen production," *International Journal of Hydrogen Energy,* vol. 43, pp. 6504-6514, 2018.

[14] J. E. Bennett, "Electrodes for generation of hydrogen and oxygen from seawater," *International Journal of Hydrogen Energy,* vol. 5, no. 4, pp. 401-408, 1980.

[15] A. A. El-Moneim, "Mn–Mo–W-oxide anodes for oxygen evolution during seawater electrolysis for hydrogen production: Effect of repeated anodic deposition," *International Journal of Hydrogen Energy,* vol. 36, no. 21, pp. 13398-13406, 2011.

[16] R. Balaji, B. S. Kannan, J. Lakshi and N. Senthil, "An alternative approach to selective sea water oxidation for hydrogen production," *Electrochemistry Communications,* vol. 11, no. 8, pp. 1700-1702, 2009.

[17] J. Mohammed-Ibrahim and H. Moussab, "Recent advances on hydrogen production through seawater electrolysis," *Materials Science for Energy Technology,* vol. 3, pp. 780-807, 2020.

[18] Y. Kuang, M. J. Kenney, Y. Meng, W.-H. Hung, Y. Liu, J. E. Huang, R. Prasanna, P. Li, Y. Li, L. Wang, M.-C. Lin, M. D. McGehee, X. Sun and H. Dai, "Solar-driven, highly sustained splitting of seawater into hydrogen and oxygen fuels," *Proceedings of the National Academy of Sciences of the United States of America,* vol. 116, no. 14, pp. 6624-6629, 2019.

[19] L. Yu, Q. Zhu, S. Song, B. McElhenny, D. Wang, C. Wu, Z. Qin, J. Bao, Y. Yu, S. Chen and Z. Ren, "Non-noble metal-nitride based electrocatalysts for high-performance alkaline seawater electrolysis," *Nature Communications,* vol. 10, no. 5106, 2019.

[20] Q. Lv, H. Jianxin, X. Tan, W. Wang, L. Cao and B. Dong, "Feather-like NiCoP Holey Nanoarrays for Efficient and Stable Seawater Splitting," *Energy Materials,* vol. 2, no. 5, pp. 3910-3917, 2019.

[21] K. Meier, "Hydrogen production with seawater electrolysis using Norwegian offshore wind energy potentials," *International Journal of Energy and Environmental Engineering,* vol. 5, no. 104, 2014.

[22] J. Brauns, J. Schonebeck, M. R. Kraglund, D. Aili, J. Hnat, J. Zitka, W. Mues, J. O. Jensen, K. Bouzek and T. Turek, "Evaluation of Diaphragms and Membranes as

Separators for Alkaline Water Electrolysis," *Journal of the Electrochemical Society,* vol. 168, no. 1, 2021.

[23] S. S. Kumar and V. Himabindu, "Hydrogen production by PEM water electrolysis – A review," *Materials Science for Energy Technologies,* vol. 2, no. 3, pp. 442-454, 2019.

[24] International Renewable Energy Agency, "Green Hydrogen Cost Reduction: Scaling Up Electrolysers to Meet the 1.5oC Goal," IRENA, Abu Dhabi, 2020.

[25] "World's largest single-stack alkaline-water electrolysis system," Internationales Verkehrswesen, 20 April 2020. [Online]. Available: https://www.internationales-verkehrswesen.de/worlds-largest-single-stack-alkaline-water-electrolysis-system/. [Accessed 1 July 2021].

[26] "Inauguration of the world's largest PEM electrolyzer," Air Liquide, 8 February 2021. [Online]. Available: https://www.airliquide.com/magazine/energy-transition/inauguration-worlds-largest-pem-electrolyzer#:~:text=Air%20Liquide%20inaugurated%20the%20largest,hydrogen%20on%20a%20large%20scale.. [Accessed 1 July 2021].

[27] Sunfire GmbH, "Renewable Hydrogen for Industrial Applications: Sunfire-Hylink SOEC," [Online]. Available: https://www.sunfire.de/files/sunfire/images/content/Sunfire.de%20(neu)/Sunfire-Factsheet-HyLink-SOEC-20210303.pdf. [Accessed 1 July 2021].

[28] A. Buttler and H. Spliethoff, "Current status of water electrolysis for energy storage, grid balancing and sector coupling via power-to-gas and power-to-liquids: A review," *Renewable and Sustainable Energy Reviews,* vol. 82, pp. 2440-2454, 2018.

[29] J. Brauns and T. Turek, "Alkaline Water Electrolysis Powered by Renewable Energy: A Review," *Processes,* vol. 8, no. 248, 2020.

[30] W. Tong, M. Forster, F. Dionigi, S. Dresp, R. S. Erami, P. Strasser, A. J. Cowan and P. Farras, "Electrolysis of low-grade and saline surface water," *Nature Energy,* vol. 5, pp. 367-377, 2020.

[31] Internationales Verkehrswesen, "World's largest single-stack alkaline-water electrolysis system," 20 April 2020. [Online]. Available: https://www.internationales-verkehrswesen.de/worlds-largest-single-stack-alkaline-water-electrolysis-system/. [Accessed 29 July 2021].

[32] Air Liquide, "Inauguration of the world's largest PEM electrolyzer," 8 February 2021. [Online]. Available: https://www.airliquide.com/magazine/energy-transition/inauguration-worlds-largest-pem-electrolyzer#:~:text=Air%20Liquide%20inaugurated%20the%20largest,hydrogen%20on%20a%20large%20scale.. [Accessed 1 July 2021].

[33] LennTech, "Composition of seawater," [Online]. Available: https://www.lenntech.com/composition-seawater.htm. [Accessed 3 August 2021].

[34] A. Altaee, G. Zaragoza and H. R. van Tonningen, “Comparison between Forward Osmosis-Reverse Osmosis and Reverse Osmosis processes for seawater desalination,” *Desalination,* vol. 336, pp. 50-57, 2014.

[35] M. E. Demir and I. Dincer, “Development of a hybrid solar thermal system with TEG and PEM electrolyzer for hydrogen and power production,” *International Journal of Hydrogen Energy,* vol. 42, pp. 30044-30056, 2017.

[36] M. Delpisheh, M. Haghghi, H. Athari and M. Mehrpooya, “Desalinated water and hydrogen generation from seawater via a desalination unit and a low temperature electrolysis using a novel solar-based setup,” *International Journal of Hydrogen Energy,* vol. 46, pp. 7211-7229, 2021.

[37] M. H. Sharqawy, M. A. Antar, S. M. Zubair and A. M. Elbashir, “Optimum thermal design of humidification dehumidification,” *Desalination,* vol. 349, pp. 10-21, 2014.

[38] O. Siddiqui and I. Dincer, “Examination of a new solar-based integrated system for desalination, electricity generation and hydrogen production,” *Solar Energy,* vol. 163, pp. 224-234, 2018.

[39] R. S. El-Emam and I. Dincer, “Thermodynamic and thermoeconomic analyses of seawater reverse osmosis desalination plant with energy recovery,” *Energy,* vol. 64, pp. 154-163, 2014.

[40] S. Kumari, R. T. White, B. Kumar and J. M. Spurgeon, “Solar hydrogen production from seawater vapour electrolysis,” *Energy & Environmental Science,* vol. 9, pp. 1725-1733, 2016.

[41] Formlabs, “Guide to Microfluidics and Millifluidics, and Lab-on-a-Chip Manufacturing,” Formlabs, [Online]. Available: https://formlabs.com/uk/blog/microfluidics-millifluidics-lab-on-a-chip-manufacturing/. [Accessed 24 July 2021].

[42] M. S. Hashemi, M. A. Modestino and D. Psaltis, “A membrane-less electrolyzer for hydrogen production across the pH scale,” *Energy & Environmental Science,* vol. 8, pp. 2003-2009, 2015.

[43] V. Schroeder, B. Emonts, H. Jansen and H. P. Schulze, “Explosion Limits of Hydrogen/Oxygen Mixtures at Initial Pressures up to 200 bar,” *Chemical Engineering Technology,* vol. 27, no. 8, pp. 847-851, 2005.

[44] S. M. H. Hashemi, J.-W. Choi, D. Psaltis and M. A. Modestino, “Membrane-less Electrolyzer”. USA Patent USPTO10,907,262, 2 February 2021.

[45] M. I. Gillespie, F. van der Merwe and R. J. Kriek, “Performance evaluation of a membraneless divergent electrode-flow-through (DEFT) alkaline electrolyser based on optimisation of electrolytic flow and electrode gap,” *Journal of Power Sources,* vol. 293, pp. 228-235, 2015.

[46] G. Anagnostopoulos, “Method and Apparatus for Producing Gas”. International Patent WO 2013/118104 A1, 15 August 2013.

[47] G. D. O'Neil, C. D. Christian, D. E. Brown and D. V. Esposito, “Hydrogen Production with a Simple and Scalable Membraneless Electrolyzer,” *Journal of the Electrochemical Society,* vol. 163, no. 11, pp. 3012-3019, 2016.

[48] J. W. Coleman and S. Garimella, “Characterization of two-phase flow patterns in small diameter round and rectangular tubes,” *International Journal of Heat and Mass Transfer,* vol. 42, pp. 2869-2881, 1999.

[49] O. O. Talabi, A. E. Dorfi, G. D. O'Neil and D. V. Esposito, “Membraneless electrolyzers for the simultaneous production of acid and base,” *Chemistry Communications,* vol. 53, pp. 8006-8009, 2017.

[50] S. Rarotra, T. K. Mandal and D. Bandyopadhyay, “Microfluidic Electrolyzers for Production and Separation of Hydrogen from Sea Water using Naturally Abundant Solar Energy,” *Energy Technology,* vol. 5, pp. 1208-1217, 2017.

[51] J. T. Davis, J. Qi, X. Fan, J. C. Bui and D. V. Esposito, “Floating membraneless PV-electrolyzer based on buoyancy-driven product separation,” *International Journal of Hydrogen Energy,* vol. 43, pp. 1224-1238, 2018.

[52] M. Hashemi, P. Karnakov, P. Hadikhani, E. Chinello, S. Litvinov, C. Moser, P. Koumoutsakos and D. Psaltis, “A versatile and membrane-less electrochemical reactor for the electrolysis of water and brine,” *Energy & Environmental Science,* vol. 12, pp. 1592-1604, 2019.

[53] B. D. Gilman, “Portable Hydrogen and Oxygen Supply System”. International Patent WO 2014/153389 A1, 25 September 2014.

[54] Gilman Industries, “Introducing Evolve,” [Online]. Available: https://gilmanindustries.com/. [Accessed 29 July 2021].

[55] B. Gilman, “C-37 EvolveTM Animation,” 23 April 2021. [Online]. Available: https://www.youtube.com/watch?v=If8JeDCnL10&t=2s. [Accessed 3 August 2021].

[56] X. Huang, S. Chang, W. S. Vincent-Lee, J. Ding and J. M. Xue, “Three-dimensional printed cellular stainless steel as a high-activity catalytic electrode for oxygen evolution,” *Journal of Materials Chemistry A,* vol. 5, no. 34, pp. 18176-18182, 2017.

[57] J. Zheng, “Pt-free NiCo electrocatalysts for oxygen evolution by seawater splitting,” *Electrochimica Acta,* vol. 247, pp. 381-391, 2017.

[58] J. Zheng, “Binary platinum alloy electrodes for hydrogen and oxygen evolutions by seawater splitting,” *Applied Surface Science,* vol. 413, pp. 72-82, 2017.

[59] F. Cheng, X. Feng, X. Chen, W. Lin, J. Rong and W. Yang, “Synergistic action of Co-Fe layered double hydroxide electrocatalyst and multiple ions of sea salt for efficient

seawater oxidation at near-neutral pH," *Electrochimica Acta*, vol. 251, pp. 336-343, 2017.

[60] Chemstations, "CHEMCAD NXT," Chemstations, 2020. [Online]. Available: https://www.chemstations.com/CHEMCAD/. [Accessed 3 August 2021].

[61] J. van Baten and R. Baur, "Cape Open to Cape Open Simulation Environment," AmsterCHEM, 2006. [Online]. Available: https://www.cocosimulator.org/. [Accessed 3 August 2021].

[62] Scottish Government, "Scotland's Marine Atlas: Information for The National Marine Plan," 16 March 2011. [Online]. Available: https://www.gov.scot/publications/scotlands-marine-atlas-information-national-marine-plan/pages/9/. [Accessed 27 July 2021].

[63] UK Government, "Offshore Energy SEA 3: Appendix 1 Environmental Baseline," [Online]. Available: https://assets.publishing.service.gov.uk/government/uploads/system/uploads/attachment_data/file/504559/OESEA3_A1f_Climate___Meteorology.pdf. [Accessed 27 July 2021].

[64] M. Telzhensky, L. Birnhack, O. Lehmann, E. Windler and O. Lahav, "Selective separation of seawater Mg2+ ions for use in downstream water treatment processes," *Chemical Engineering Journal*, vol. 175, pp. 136-143, 2011.

[65] V. Belessiotis, S. Kalogirou and E. Delyannis, "Humidification-Dehumidification," in *Thermal Solar Desalination: Methods and Systems*, Academic Press, 2016, pp. 253-281.

[66] D. V. Esposito and G. D. O'Neil, "Membraneless Electrochemical Flow-Through Reactor". United States of America Patent US 20170081770A1 , 23 March 2017.

[67] H. M. Arain, "Water Properties Calculator," Hamza's Reef, [Online]. Available: https://www.hamzasreef.com/Contents/Calculators/WaterProperties.php. [Accessed 27 July 2021].

[68] The Engineering ToolBox, "Fluid Heat Transfer Coefficients: Heat Exchanger Surface Combinations," Engineering Toolbox, 2003. [Online]. Available: https://www.engineeringtoolbox.com/overall-heat-transfer-coefficients-d_284.html. [Accessed 3 August 2021].

[69] International Finance Corporation, "General EHS Guidelines: Environmental, Wastewater and Ambient Water Quality," 30 April 2007. [Online]. Available: https://www.ifc.org/wps/wcm/connect/3d9a54ae-c44c-488d-9851-afeb368cb9f9/1-3%2BWastewater%2Band%2BAmbient%2BWater%2BQuality.pdf?MOD=AJPERES&CVID=ls4Xbfn. [Accessed 26 July 2021].

[70] S. P. Knaebel, D. Ko and L. T. Biegler, "Simulation and Optimization of a Pressure Swing Adsorption System: Recovering Hydrogen from Methane," *Adsorption,* vol. 11, pp. 615-620, 2005.

[71] A. Bahadori, "Chapter 4: Gas-Liquid Separators," in *Natural Gas Processing: Technology and Engineering Design*, Gulf Professional Publishing, 2014, pp. 151-222.

[72] Engineering ToolBox, "Air - Composition and Molecular Weight," Engineering ToolBox, 2003. [Online]. Available: https://www.engineeringtoolbox.com/air-composition-d_212.html. [Accessed 3 August 2021].

[73] R. C. Ropp, "Chapter 3 - Group 16 (O, S, Se, Te) Alkaline Earth Compounds," in *Encyclopedia of the Alkaline Earth Compounds*, Elsevier, 2013, pp. 105-197.

[74] R. K. Sinnott, "Chapter 10: Equipment Selection, Specification and Design," in *Chemical Engineering Design: Volume 6*, Oxford, Elsevier, 2005, pp. 400-492.

[75] M. T. Schobeiri, "Modeling the Compressor Component, Design and Off-Design," in *Gas Turbine Design, Components and System Design Integration*, Springer, 2018, pp. 369-425.

[76] X. Shi, X. Liao and Y. Li, "Quantification of fresh water consumption and scarcity footprints of hydrogen from water electrolysis: A methodology framework," *Renewable Energy*, vol. 154, pp. 786-796, 2020.

[77] J. G. Speight, "Chapter 8 - Corrosion," in *Subsea and Deepwater Oil and Gas Science and Technology*, Wyoming, Gulf Professional Publishing, 2015, pp. 213-256.

[78] K. A. Chandler, "Introduction: The control of corrosion in marine environments," in *Marine and Offshore Corrosion: Marine Engineering Series*, Elsevier Science and Technology, 1984, pp. 1-7.

[79] T. Bacquart, A. Murugan, M. Carre, B. Gozlan, F. Aupretre, F. Haloua and T. A. Aarhaug, "Probability of occurrence of ISO 14687-2 contaminants in hydrogen: Principles and examples from steam methane reforming and electrolysis (water and chlor-alkali) production processes model," *International Journal of Hydrogen Energy*, vol. 43, pp. 11872-11883, 2018.

[80] Research and Markets, "Global Magnesium Hydroxide Market Report 2020: $773 Million Market Opportunities, Trends, Forecast and Competitive Analysis to 2025," Cision PR Newswire, 8 October 2020. [Online]. Available: https://www.prnewswire.com/news-releases/global-magnesium-hydroxide-market-report-2020-773-million-market-opportunities-trends-forecast-and-competitive-analysis-to-2025-301148491.html. [Accessed 14 August 2021].

[81] Market Watch, "Silicon Dioxide Market 2021: Global Companies by Size, Growth of Manufacturers, Research Findings, and Regional Opportunities Forecast to 2030," Market Watch, 23 June 2021. [Online]. Available: https://www.marketwatch.com/press-release/silicon-dioxide-market-2021-global-

companies-by-size-growth-of-manufacturers-research-findings-and-regional-opportunities-forecast-to-2030-2021-06-23. [Accessed 14 August 2021].

[82] A. Giwa, N. Akther, A. Al Housani, S. Haris and S. W. Hasan, “Recent advances in humidification dehumidification (HDH),” *Renewable and Sustainable Energy Reviews*, vol. 57, pp. 929-944, 2016.

[83] F. Scheepers, M. Stahler, A. Stahler, E. Rauls, M. Muller, M. Carmo and W. Lehnert, “Improving the Efficiency of PEM Electrolyzers through Membrane-Specific Pressure Optimization,” *Energies*, vol. 13, no. 612, 2020.

Appendix 1: Mass and Energy Balances

Process 1 (Alkaline)

Component	MW (g/mol)	S100	S110	S120	S130	S140	S150	S200
H_2O	18.02	87.94	87.94	87.94	52.11	52.11	458.95	79.14
H_2	2.02	0.00	0.00	0.00	0.00	0.00	0.00	0.00
O_2	32.00	0.00	0.00	0.00	0.00	0.00	0.00	0.00
NaOH	40.00	0.00	0.00	0.00	0.00	0.00	0.00	0.00
Cl^-	35.45	1.67	1.67	1.67	0.00	0.00	0.00	0.47
Na^+	22.99	0.93	0.93	0.93	0.00	0.00	0.00	0.04
SO_4^{2-}	96.06	0.23	0.23	0.23	0.00	0.00	0.00	0.23
Mg^{2+}	24.31	0.11	0.11	0.11	0.00	0.00	0.00	0.11
Ca^{2+}	40.08	0.04	0.04	0.04	0.00	0.00	0.00	0.04
K^+	39.10	0.03	0.03	0.03	0.00	0.00	0.00	0.01
HCO^{3-}	61.02	0.01	0.01	0.01	0.00	0.00	0.00	0.00
Sr^{2+}	87.62	0.00	0.00	0.00	0.00	0.00	0.00	0.00
Br^-	79.90	0.01	0.01	0.01	0.00	0.00	0.00	0.01
BO_3^{3-}	58.81	0.00	0.00	0.00	0.00	0.00	0.00	0.00
NaCl	58.44	0.00	0.00	0.00	0.00	0.00	0.00	0.00
TOTAL (kg/h)		90.97	90.97	90.97	52.11	52.11	458.95	80.06
	Salinity (ppt)	34.47	34.47	34.47	0.00	0.00	0.00	11.60
	P (bara)	1.01	15.01	15.01	1.01	1.01	1.01	1.01
	T (°C)	5.00	5.00	25.00	100.00	26.00	78.72	25.00
	T (K)	278.15	278.15	298.15	373.15	299.15	351.87	298.15
	T_{ref} (K)	273.15	273.15	273.15	273.15	273.15	273.15	273.15
	C_P (kJ/kg.K)	4.00	4.00	4.00	1.89	1.89	4.18	4.12
	Q (kW)	0.50	0.50	2.53	2.74	0.71	41.95	2.29

Component	MW (g/mol)	S300	S400	S500	S600	S610	S620	S630
H_2O	18.02	8.79	0.00	15.57	6.64	6.64	590.14	590.14
H_2	2.02	0.00	0.00	0.00	0.00	0.00	0.00	0.00
O_2	32.00	0.00	0.00	0.00	0.00	0.00	0.00	0.00
NaOH	40.00	0.00	0.00	6.23	6.23	6.23	0.00	0.00
Cl^-	35.45	1.20	0.00	0.05	0.05	0.05	11.20	11.20
Na^+	22.99	0.89	0.00	0.09	0.09	0.09	6.23	6.23
SO_4^{2-}	96.06	0.00	0.00	0.00	0.00	0.00	1.56	1.56
Mg^{2+}	24.31	0.00	0.00	0.00	0.00	0.00	0.74	0.74
Ca^{2+}	40.08	0.00	0.00	0.00	0.00	0.00	0.24	0.24
K^+	39.10	0.02	0.00	0.02	0.02	0.02	0.22	0.22
HCO^{3-}	61.02	0.01	0.00	0.01	0.01	0.01	0.08	0.08
Sr^{2+}	87.62	0.00	0.00	0.00	0.00	0.00	0.01	0.01
Br^-	79.90	0.00	0.00	0.00	0.00	0.00	0.04	0.04
BO_3^{3-}	58.81	0.00	0.00	0.00	0.00	0.00	0.02	0.02
NaCl	58.44	0.00	1.88	0.00	0.00	0.00	0.00	0.00
TOTAL (kg/h)		10.91	1.88	21.98	13.04	13.04	610.48	610.48
	Salinity (ppt)	240.35	N/A	411.36	964.78	964.78	34.47	34.47
	P (bara)	1.01	1.01	1.01	1.01	1.01	1.01	1.01
	T (ºC)	25.00	25.00	25.00	70.00	25.00	5.00	8.00
	T (K)	298.15	298.15	298.15	343.15	298.15	278.15	281.15
	T_{ref} (K)	273.15	273.15	273.15	273.15	273.15	273.15	273.15
	C_P (kJ/kg.K)	3.37	0.00	3.38	12.47	12.47	4.00	4.00
	Q (kW)	0.26	0.00	0.52	3.16	1.13	3.39	5.42

Component	MW (g/mol)	S700	S710	S800	S810
H_2O	18.02	0.00	0.00	0.00	0.00
H_2	2.02	0.00	0.00	1.00	1.00
O_2	32.00	7.93	7.93	0.00	0.00
NaOH	40.00	0.00	0.00	0.00	0.00
Cl^-	35.45	0.00	0.00	0.00	0.00
Na^+	22.99	0.00	0.00	0.00	0.00
SO_4^{2-}	96.06	0.00	0.00	0.00	0.00
Mg^{2+}	24.31	0.00	0.00	0.00	0.00
Ca^{2+}	40.08	0.00	0.00	0.00	0.00
K^+	39.10	0.00	0.00	0.00	0.00
HCO^{3-}	61.02	0.00	0.00	0.00	0.00
Sr^{2+}	87.62	0.00	0.00	0.00	0.00
Br^-	79.90	0.00	0.00	0.00	0.00
BO_3^{3-}	58.81	0.00	0.00	0.00	0.00
NaCl	58.44	0.00	0.00	0.00	0.00
TOTAL (kg/h)		7.93	7.93	1.00	1.00
	Salinity (ppt)	N/A	N/A	N/A	N/A
	P (bara)	30.00	200.00	30.00	350.00
	T (^{o}C)	70.00	475.24	70.00	366.80
	T (K)	343.15	748.39	343.15	639.95
	T_{ref} (K)	273.15	273.15	273.15	273.15
	C_P (kJ/kg.K)	0.92	0.92	14.30	14.30
	Q (kW)	0.14	0.96	0.28	1.46

Process 2 (PEM 1)

Component	MW (g/mol)	S100	S110	S120	S200	S210	S220	S230
H_2O	18.02	11959.18	11959.18	0.16	11939.51	11950.40	11950.40	289403.39
H_2	2.02	0.00	0.00	0.00	0.00	0.00	0.00	0.00
O_2	32.00	0.00	0.00	8.33	0.00	0.00	0.00	0.00
N_2	28.01	0.00	0.00	27.17	0.00	0.00	0.00	0.00
CO_2	44.01	0.00	0.00	0.02	0.00	0.00	0.00	0.00
Ar	39.95	0.00	0.00	0.46	0.00	0.00	0.00	0.00
Cl^-	35.45	226.99	226.99	0.00	226.99	226.99	226.99	5492.88
Na^+	22.99	126.24	126.24	0.00	126.24	126.24	126.24	3054.94
SO_4^{2-}	96.06	31.68	31.68	0.00	31.68	31.68	31.68	766.63
Mg^{2+}	24.31	15.09	15.09	0.00	15.09	15.09	15.09	365.23
Ca^{2+}	40.08	4.78	4.78	0.00	4.78	4.78	4.78	115.76
K^+	39.10	4.54	4.54	0.00	4.54	4.54	4.54	109.97
HCO^{3-}	61.02	1.67	1.67	0.00	1.67	1.67	1.67	40.52
Sr^{2+}	87.62	0.16	0.16	0.00	0.16	0.16	0.16	3.76
Br^-	79.90	0.78	0.78	0.00	0.78	0.78	0.78	18.81
BO_3^{3-}	58.81	0.31	0.31	0.00	0.31	0.31	0.31	7.52
TOTAL		12371.43	12371.43	36.14	12351.75	12362.64	12362.64	299379.42
	Salinity (ppt)	34.47	34.47	N/A	34.53	34.50	34.50	34.47
	P (bara)	1.01	2.00	1.01	1.01	1.01	1.01	1.01
	T (^{o}C)	5.00	5.00	5.00	80.00	79.99	8.00	5.00
	T (K)	278.15	278.15	278.15	353.15	353.14	281.15	278.15
	T_{ref} (K)	273.15	273.15	273.15	273.15	273.15	273.15	273.15
	C_P (kJ/kg.K)	4.00	4.00	1.02	4.00	4.03	4.00	4.00
	Q (kW)	68.66	68.66	0.05	1096.84	1106.74	109.81	1661.56

Component	MW (g/mol)	S240	S300	S400	S500	S510	S520	S600
H_2O	18.02	289403.39	19.83	0.00	10.89	10.89	0.00	0.00
H_2	2.02	0.00	0.00	0.00	0.00	0.00	0.00	1.00
O_2	32.00	0.00	8.33	0.00	7.94	0.00	7.94	0.00
N_2	28.01	0.00	27.17	17.28	27.17	0.00	27.17	17.28
CO_2	44.01	0.00	0.02	0.00	0.02	0.00	0.02	0.00
Ar	39.95	0.00	0.46	0.00	0.46	0.00	0.46	0.00
Cl^-	35.45	5492.88	0.00	0.00	0.00	0.00	0.00	0.00
Na^+	22.99	3054.94	0.00	0.00	0.00	0.00	0.00	0.00
SO_4^{2-}	96.06	766.63	0.00	0.00	0.00	0.00	0.00	0.00
Mg^{2+}	24.31	365.23	0.00	0.00	0.00	0.00	0.00	0.00
Ca^{2+}	40.08	115.76	0.00	0.00	0.00	0.00	0.00	0.00
K^+	39.10	109.97	0.00	0.00	0.00	0.00	0.00	0.00
HCO^{3-}	61.02	40.52	0.00	0.00	0.00	0.00	0.00	0.00
Sr^{2+}	87.62	3.76	0.00	0.00	0.00	0.00	0.00	0.00
Br^-	79.90	18.81	0.00	0.00	0.00	0.00	0.00	0.00
BO_3^{3-}	58.81	7.52	0.00	0.00	0.00	0.00	0.00	0.00
TOTAL		299379.42	55.82	17.28	46.49	10.89	35.60	18.28
	Salinity (ppt)	34.47	N/A	N/A	N/A	0.00	N/A	N/A
	P (bara)	1.01	1.01	1.01	30.00	1.01	1.01	30.00
	T (ºC)	8.00	80.00	70.00	70.00	70.00	70.00	70.00
	T (K)	281.15	353.15	343.15	343.15	343.15	343.15	343.15
	T_{ref} (K)	273.15	273.15	273.15	273.15	273.15	273.15	273.15
	C_P (kJ/kg.K)	4.00	2.13	1.04	1.75	4.18	1.01	1.77
	Q (kW)	2658.49	2.65	0.35	1.58	0.89	0.70	0.63

Component	MW (g/mol)	S800	S810
H_2O	18.02	0.00	0.00
H_2	2.02	1.00	1.00
O_2	32.00	0.00	0.00
N_2	28.01	0.00	0.00
CO_2	44.01	0.00	0.00
Ar	39.95	0.00	0.00
Cl^-	35.45	0.00	0.00
Na^+	22.99	0.00	0.00
SO_4^{2-}	96.06	0.00	0.00
Mg^{2+}	24.31	0.00	0.00
Ca^{2+}	40.08	0.00	0.00
K^+	39.10	0.00	0.00
HCO^{3-}	61.02	0.00	0.00
Sr^{2+}	87.62	0.00	0.00
Br^-	79.90	0.00	0.00
BO_3^{3-}	58.81	0.00	0.00
TOTAL		1.00	1.00
	Salinity (ppt)	N/A	N/A
	P (bara)	30.00	350.00
	T (^oC)	70.00	490.46
	T (K)	343.15	763.61
	T_{ref} (K)	273.15	273.15
	C_P (kJ/kg.K)	14.30	14.30
	Q (kW)	0.28	1.95

Process 3 (PEM 2)

Component	MW (g/mol)	S100	S150	S200	S300	S400	S500	S600
H_2O	18.02	32.43	32.43	23.41	9.03	0.00	9.03	19.83
H_2	2.02	0.00	0.00	0.00	0.00	0.00	0.00	0.00
O_2	32.00	0.00	0.00	0.00	7.51	7.51	0.00	0.00
N_2	28.01	0.00	0.00	0.00	24.49	24.49	0.00	0.00
CO_2	44.01	0.00	0.00	0.00	0.02	0.02	0.00	0.00
Ar	39.95	0.00	0.00	0.00	0.42	0.42	0.00	0.00
Cl^-	35.45	0.62	0.62	0.62	0.00	0.00	0.00	0.00
Na^+	22.99	0.34	0.34	0.34	0.00	0.00	0.00	0.00
SO_4^{2-}	96.06	0.09	0.09	0.09	0.00	0.00	0.00	0.00
Mg^{2+}	24.31	0.04	0.04	0.04	0.00	0.00	0.00	0.00
Ca^{2+}	40.08	0.01	0.01	0.01	0.00	0.00	0.00	0.00
K^+	39.10	0.01	0.01	0.01	0.00	0.00	0.00	0.00
HCO^{3-}	61.02	0.00	0.00	0.00	0.00	0.00	0.00	0.00
Sr^{2+}	87.62	0.00	0.00	0.00	0.00	0.00	0.00	0.00
Br^-	79.90	0.00	0.00	0.00	0.00	0.00	0.00	0.00
BO_3^{3-}	58.81	0.00	0.00	0.00	0.00	0.00	0.00	0.00
TOTAL (kg/h)		33.55	33.55	24.52	41.46	32.43	9.03	19.83
	Salinity (ppt)	34.47	34.47	47.76	N/A	N/A	0.00	0.00
	P (bara)	1.01	2.00	1.01	1.01	1.01	1.01	1.01
	T (^{o}C)	5.00	5.00	80.00	80.00	80.00	80.00	78.22
	T (K)	278.15	278.15	353.15	353.15	353.15	353.15	351.37
	T_{ref} (K)	273.15	273.15	273.15	273.15	273.15	273.15	273.15
	C_P (kJ/kg.K)	4.00	4.00	3.97	1.70	1.00	4.18	4.18
	Q (kW)	0.19	0.19	2.16	1.56	0.72	0.84	1.80

Component	MW (g/mol)	S700	S710	S800	S900	S910	S920	S930
H_2O	18.02	0.00	0.00	10.89	0.00	0.00	10.98	1.96
H_2	2.02	1.00	1.00	0.00	0.00	0.00	0.00	0.00
O_2	32.00	0.00	0.00	7.94	7.94	7.94	0.00	0.00
N_2	28.01	0.00	0.00	0.00	0.00	0.00	0.00	0.00
CO_2	44.01	0.00	0.00	0.00	0.00	0.00	0.00	0.00
Ar	39.95	0.00	0.00	0.00	0.00	0.00	0.00	0.00
Cl^-	35.45	0.00	0.00	0.00	0.00	0.00	0.00	0.00
Na^+	22.99	0.00	0.00	0.00	0.00	0.00	0.00	0.00
SO_4^{2-}	96.06	0.00	0.00	0.00	0.00	0.00	0.00	0.00
Mg^{2+}	24.31	0.00	0.00	0.00	0.00	0.00	0.00	0.00
Ca^{2+}	40.08	0.00	0.00	0.00	0.00	0.00	0.00	0.00
K^+	39.10	0.00	0.00	0.00	0.00	0.00	0.00	0.00
HCO^{3-}	61.02	0.00	0.00	0.00	0.00	0.00	0.00	0.00
Sr^{2+}	87.62	0.00	0.00	0.00	0.00	0.00	0.00	0.00
Br^-	79.90	0.00	0.00	0.00	0.00	0.00	0.00	0.00
BO_3^{3-}	58.81	0.00	0.00	0.00	0.00	0.00	0.00	0.00
TOTAL (kg/h)		1.00	1.00	18.83	7.94	7.94	10.98	1.96
	Salinity (ppt)	N/A	N/A	0.00	N/A	N/A	0.00	0.00
	P (bara)	30.00	350.00	30.00	1.01	200.00	1.01	1.01
	T (ºC)	70.00	366.80	70.00	70.00	1775.92	70.00	70.00
	T (K)	343.15	639.95	343.15	343.15	2049.07	343.15	343.15
	T_{ref} (K)	273.15	273.15	273.15	273.15	273.15	273.15	273.15
	C_P (kJ/kg.K)	14.30	14.30	2.80	0.92	0.92	4.18	4.18
	Q (kW)	0.28	1.46	1.03	0.14	3.59	0.89	0.16

Component	MW (g/mol)	S940	S1000	S1010	S1020	S1030
H_2O	18.02	9.03	32.43	32.43	754.57	754.57
H_2	2.02	0.00	0.00	0.00	0.00	0.00
O_2	32.00	0.00	0.00	0.00	0.00	0.00
N_2	28.01	0.00	0.00	0.00	0.00	0.00
CO_2	44.01	0.00	0.00	0.00	0.00	0.00
Ar	39.95	0.00	0.00	0.00	0.00	0.00
Cl^-	35.45	0.00	0.62	0.62	14.32	14.32
Na^+	22.99	0.00	0.34	0.34	7.97	7.97
SO_4^{2-}	96.06	0.00	0.09	0.09	2.00	2.00
Mg^{2+}	24.31	0.00	0.04	0.04	0.95	0.95
Ca^{2+}	40.08	0.00	0.01	0.01	0.30	0.30
K^+	39.10	0.00	0.01	0.01	0.29	0.29
HCO^{3-}	61.02	0.00	0.00	0.00	0.11	0.11
Sr^{2+}	87.62	0.00	0.00	0.00	0.01	0.01
Br^-	79.90	0.00	0.00	0.00	0.05	0.05
BO_3^{3-}	58.81	0.00	0.00	0.00	0.02	0.02
TOTAL (kg/h)		9.03	33.55	33.55	780.58	780.58
	Salinity (ppt)	0.00	34.47	34.47	34.47	34.47
	P (bara)	1.01	1.01	1.01	1.01	1.01
	T (ºC)	70.00	77.21	8.00	5.00	8.00
	T (K)	343.15	350.36	281.15	278.15	281.15
	T_{ref} (K)	273.15	273.15	273.15	273.15	273.15
	C_P (kJ/kg.K)	4.18	4.03	4.00	4.00	4.00
	Q (kW)	0.73	2.90	0.30	4.33	6.93

Process 4 (Membrane-less)

Component	MW (g/mol)	S100	S110	S111	S112	S120	S300	S400
H_2O	18.02	21859.84	21859.84	9091.69	9091.69	21859.84	21859.84	36233.44
H_2	2.02	0.00	0.00	0.00	0.00	0.00	0.00	0.00
O_2	32.00	0.00	0.00	0.00	0.00	0.00	0.00	0.00
Cl^-	35.45	414.90	414.90	0.00	0.00	414.90	414.90	687.71
Na^+	22.99	230.75	230.75	0.00	0.00	230.75	230.75	382.48
SO_4^{2-}	96.06	57.91	57.91	0.00	0.00	57.91	57.91	95.98
Mg^{2+}	24.31	27.59	27.59	0.00	0.00	27.59	27.59	0.00
Ca^{2+}	40.08	8.74	8.74	0.00	0.00	8.74	8.74	14.49
K^+	39.10	8.31	8.31	0.00	0.00	8.31	8.31	13.77
HCO^{3-}	61.02	3.06	3.06	0.00	0.00	3.06	3.06	5.07
Sr^{2+}	87.62	0.28	0.28	0.00	0.00	0.28	0.28	0.47
Br^-	79.90	1.42	1.42	0.00	0.00	1.42	1.42	2.36
BO_3^{3-}	58.81	0.57	0.57	0.00	0.00	0.57	0.57	0.94
$Mg(OH)_2$	57.00	0.00	0.00	0.00	0.00	0.00	0.00	64.70
OH^-	17.01	0.00	0.00	0.00	0.00	0.00	0.00	0.60
H^+	1.01	0.00	0.00	0.00	0.00	0.00	0.00	0.00
Mg_2SiO_4	140.69	0.00	0.00	0.00	0.00	0.00	0.00	0.00
SiO_2	60.08	0.00	0.00	0.00	0.00	0.00	0.00	0.00
TOTAL		22613.37	22613.37	9091.69	9091.69	22613.37	22613.37	37502.02
	Salinity (ppt)	34.47	34.47	0.00	0.00	34.47	34.47	33.21
	P (bara)	1.01	2.00	1.01	1.01	2.00	1.01	1.01
	T (°C)	5.00	5.00	100.00	21.00	20.00	20.00	57.03
	T (K)	278.15	278.15	373.15	294.15	293.15	293.15	330.18
	T_{ref} (K)	273.15	273.15	273.15	273.15	273.15	273.15	273.15
	C_P (kJ/kg.K)	4.00	4.00	1.89	1.89	4.00	4.00	4.01
	Q (kW)	125.50	125.69	477.31	100.24	502.77	502.77	2381.27

Component	MW (g/mol)	S500	S600	S700	S800	S900	S1000	S1010
H_2O	18.02	0.00	36233.44	29263.94	6969.50	14611.52	281.51	281.51
H_2	2.02	0.00	0.00	0.00	0.00	0.00	0.00	0.00
O_2	32.00	0.00	0.00	0.00	0.00	0.00	0.00	0.00
Cl^-	35.45	0.00	687.71	555.43	132.28	277.33	5.34	5.34
Na^+	22.99	0.00	382.48	308.91	73.57	154.24	2.97	2.97
SO_4^{2-}	96.06	0.00	95.98	77.52	18.46	38.71	0.75	0.75
Mg^{2+}	24.31	0.00	0.00	0.00	0.00	0.00	0.00	0.00
Ca^{2+}	40.08	0.00	14.49	11.71	2.79	5.84	0.11	0.11
K^+	39.10	0.00	13.77	11.12	2.65	5.55	0.11	0.11
HCO^{3-}	61.02	0.00	5.07	4.10	0.98	2.05	0.04	0.04
Sr^{2+}	87.62	0.00	0.47	0.38	0.09	0.19	0.00	0.00
Br^-	79.90	0.00	2.36	1.90	0.45	0.95	0.02	0.02
BO_3^{3-}	58.81	0.00	0.94	0.76	0.18	0.38	0.01	0.01
$Mg(OH)_2$	57.00	64.70	0.00	0.00	0.00	0.00	0.00	0.00
OH^-	17.01	0.00	0.60	0.49	0.12	38.62	0.51	0.51
H^+	1.01	0.00	0.00	0.00	0.00	0.00	0.00	0.00
Mg_2SiO_4	140.69	0.00	0.00	0.00	0.00	0.00	0.00	0.00
SiO_2	60.08	0.00	0.00	0.00	0.00	0.00	0.00	0.00
TOTAL		64.70	37437.32	30236.25	7201.07	15135.37	291.37	291.37
	Salinity (ppt)	N/A	33.21	33.21	33.21	33.21	33.21	33.21
	P (bara)	1.01	1.01	1.01	1.01	1.01	1.01	10.00
	T (^{o}C)	57.03	57.03	57.03	57.03	50.00	50.00	50.00
	T (K)	330.18	330.18	330.18	330.18	323.15	323.15	323.15
	T_{ref} (K)	273.15	273.15	273.15	273.15	273.15	273.15	273.15
	C_P (kJ/kg.K)	1.35	4.01	4.01	4.01	4.02	4.02	4.02
	Q (kW)	1.39	2379.92	1922.14	457.78	844.85	16.26	16.26

Component	MW (g/mol)	S1100	S1200	S1210	S1220	S1230	S1240	S1300
H_2O	18.02	14330.01	14611.52	0.00	14631.65	0.00	14631.65	87.50
H_2	2.02	0.00	0.00	0.00	0.00	0.00	0.00	0.00
O_2	32.00	0.00	0.00	0.00	0.00	0.00	0.00	8.05
Cl^-	35.45	271.98	277.33	0.00	277.33	0.00	277.33	2.67
Na^+	22.99	151.27	154.24	0.00	154.24	0.00	154.24	1.49
SO_4^{2-}	96.06	37.96	38.71	0.00	38.71	0.00	38.71	0.37
Mg^{2+}	24.31	0.00	0.00	0.00	27.16	0.00	27.16	0.00
Ca^{2+}	40.08	5.73	5.84	0.00	5.84	0.00	5.84	0.06
K^+	39.10	5.45	5.55	0.00	5.55	0.00	5.55	0.05
HCO^{3-}	61.02	2.01	2.05	0.00	2.05	0.00	2.05	0.02
Sr^{2+}	87.62	0.19	0.19	0.00	0.19	0.00	0.19	0.00
Br^-	79.90	0.93	0.95	0.00	0.95	0.00	0.95	0.01
BO_3^{3-}	58.81	0.37	0.38	0.00	0.38	0.00	0.38	0.00
$Mg(OH)_2$	57.00	0.00	0.00	0.00	0.00	0.00	0.00	0.00
OH^-	17.01	38.11	0.00	0.00	0.00	0.00	0.00	0.24
H^+	1.01	0.00	2.29	0.00	0.04	0.00	0.04	0.00
Mg_2SiO_4	140.69	0.00	0.00	78.62	0.00	0.00	0.00	0.00
SiO_2	60.08	0.00	0.00	0.00	33.57	33.57	0.00	0.00
TOTAL		14844.00	15099.04	78.62	15177.66	33.57	15144.08	100.46
	Salinity (ppt)	33.21	33.21	N/A	35.02	N/A	35.02	53.42
	P (bara)	1.01	1.01	1.01	1.01	1.01	1.01	10.00
	T (^oC)	50.00	50.00	25.00	54.16	54.16	54.16	80.00
	T (K)	323.15	323.15	298.15	327.31	327.31	327.31	353.15
	T_{ref} (K)	273.15	273.15	273.15	273.15	273.15	273.15	273.15
	C_P (kJ/kg.K)	4.02	4.02	0.85	4.00	0.73	4.01	3.70
	Q (kW)	828.58	842.82	0.46	913.94	0.37	913.57	8.25

Component	MW (g/mol)	S1400	S1500	S1600	S1700	S1800	S1900	S1910
H_2O	18.02	0.00	87.50	87.50	87.50	0.00	21776.79	342107.37
H_2	2.02	0.00	0.00	1.00	0.00	1.00	0.00	0.00
O_2	32.00	8.05	0.00	0.00	0.00	0.00	0.00	0.00
Cl^-	35.45	0.00	2.67	2.67	2.67	0.00	413.19	6493.20
Na^+	22.99	0.00	1.49	1.49	1.49	0.00	229.75	3611.29
SO_4^{2-}	96.06	0.00	0.37	0.37	0.37	0.00	57.91	906.24
Mg^{2+}	24.31	0.00	0.00	0.00	0.00	0.00	27.16	431.74
Ca^{2+}	40.08	0.00	0.06	0.06	0.06	0.00	8.75	136.84
K^+	39.10	0.00	0.05	0.05	0.05	0.00	8.31	130.00
HCO^{3-}	61.02	0.00	0.02	0.02	0.02	0.00	3.06	47.90
Sr^{2+}	87.62	0.00	0.00	0.00	0.00	0.00	0.28	4.45
Br^-	79.90	0.00	0.01	0.01	0.01	0.00	1.42	22.24
BO_3^{3-}	58.81	0.00	0.00	0.00	0.00	0.00	0.57	0.00
$Mg(OH)_2$	57.00	0.00	0.00	0.00	0.00	0.00	0.00	0.00
OH^-	17.01	0.00	0.24	0.24	0.24	0.00	0.00	0.00
H^+	1.01	0.00	0.00	0.00	0.00	0.00	0.00	0.00
Mg_2SiO_4	140.69	0.00	0.00	0.00	0.00	0.00	0.00	0.00
SiO_2	60.08	0.00	0.00	0.00	0.00	0.00	0.00	0.00
TOTAL		8.05	92.41	93.41	92.41	1.00	22527.19	353891.26
	Salinity (ppt)	N/A	53.42	53.42	53.42	N/A	34.46	34.47
	P (bara)	1.01	10.00	10.00	10.00	10.00	1.01	1.01
	T (^oC)	80.00	80.00	80.00	80.00	80.00	55.10	5.00
	T (K)	353.15	353.15	353.15	353.15	353.15	328.25	278.15
	T_{ref} (K)	273.15	273.15	273.15	273.15	273.15	273.15	273.15
	C_P (kJ/kg.K)	0.92	3.95	4.05	3.95	14.30	4.01	4.00
	Q (kW)	0.16	8.11	8.40	8.11	0.32	1383.01	1964.10

Component	MW (g/mol)	S1920	S2000
H_2O	18.02	342107.37	21776.79
H_2	2.02	0.00	0.00
O_2	32.00	0.00	0.00
Cl^-	35.45	6493.20	413.19
Na^+	22.99	3611.29	229.75
SO_4^{2-}	96.06	906.24	57.91
Mg^{2+}	24.31	431.74	27.16
Ca^{2+}	40.08	136.84	8.75
K^+	39.10	130.00	8.31
HCO^{3-}	61.02	47.90	3.06
Sr^{2+}	87.62	4.45	0.28
Br^-	79.90	22.24	1.42
BO_3^{3-}	58.81	0.00	0.57
$Mg(OH)_2$	57.00	0.00	0.00
OH^-	17.01	0.00	0.00
H^+	1.01	0.00	0.00
Mg_2SiO_4	140.69	0.00	0.00
SiO_2	60.08	0.00	0.00
TOTAL		353891.26	22527.19
	Salinity (ppt)	34.47	34.47
	P (bara)	1.01	1.01
	T (^oC)	8.00	8.00
	T (K)	281.15	281.15
	T_{ref} (K)	273.15	273.15
	C_P (kJ/kg.K)	4.00	4.00
	Q (kW)	3147.27	200.04

Appendix 2: J-V Graphs

Device No. 1

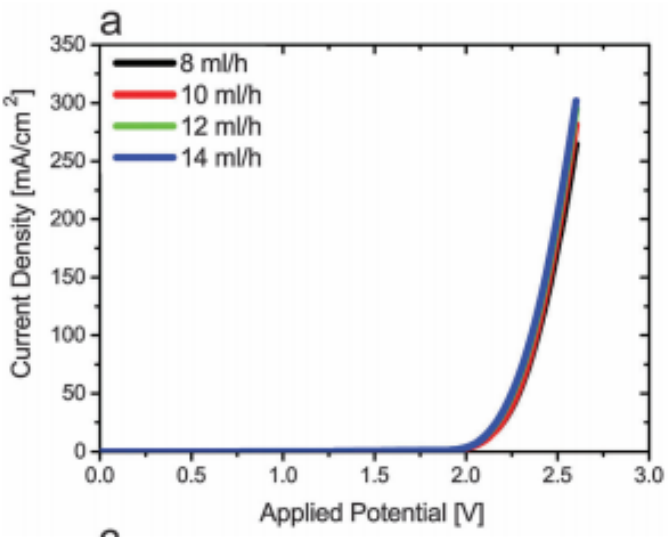

Figure 23 - Current density plotted against cell voltage (J-V) for Membrane-less Device No. 1, taken from [42].

Device No. 2

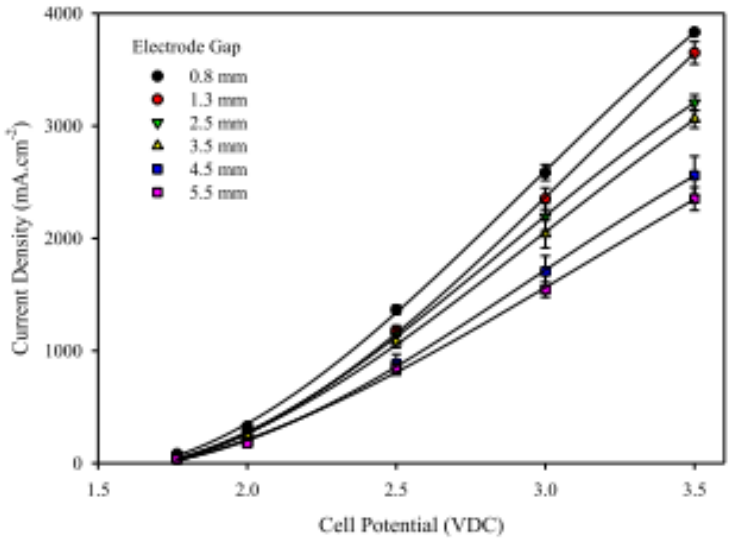

Figure 24 - Current density plotted against cell voltage (J-V) for Membrane-less Device No. 2, taken from [45].

Device No. 3

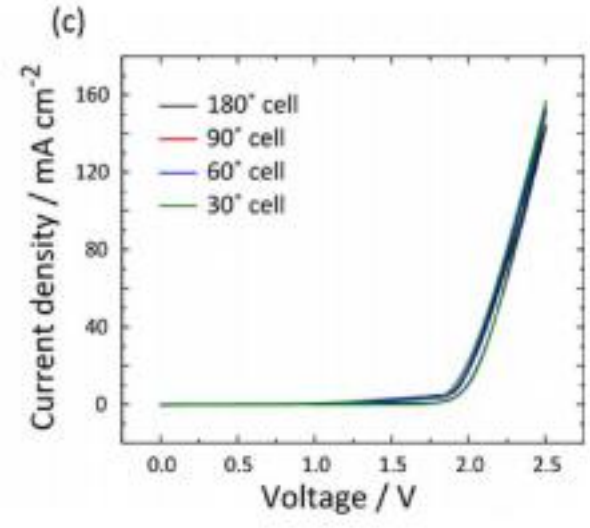

Figure 25 - Current density plotted against cell voltage (J-V) for Membrane-less Device No. 3, taken from [47].

Device No. 4

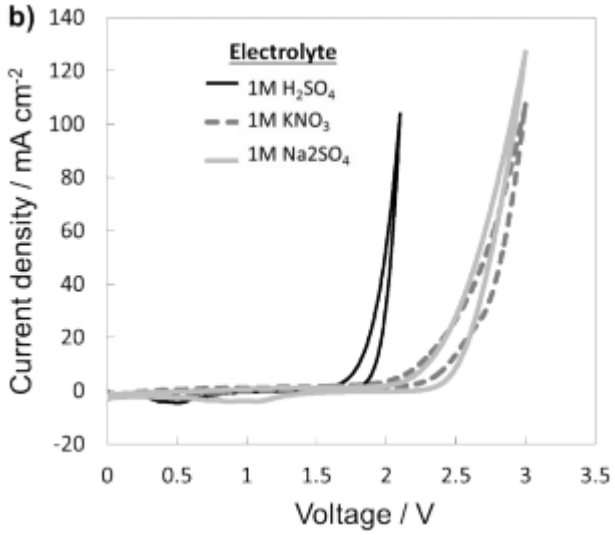

Figure 26 - Current density plotted against cell voltage (J-V) for Membrane-less Device No. 4, taken from supplementary information of [49].

Device No. 6

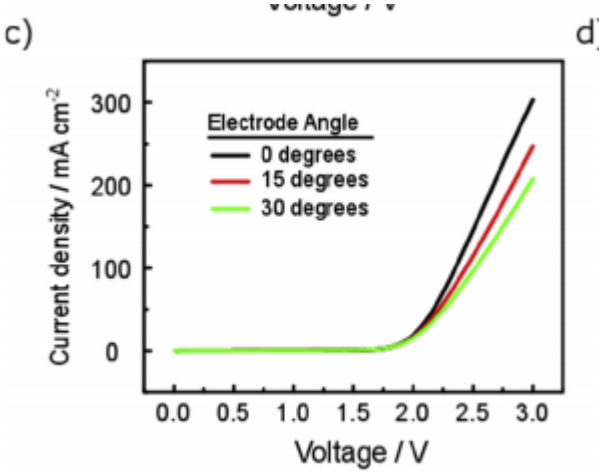

Figure 27 - Current density plotted against cell voltage (J-V) for Membrane-less Device No. 6, taken from [51].

Appendix 3: Relationship Between Flow Regime/Electrode Separation Distance and Cell Efficiency Graphs

Electrode Separation Distance Versus HHV Efficiency

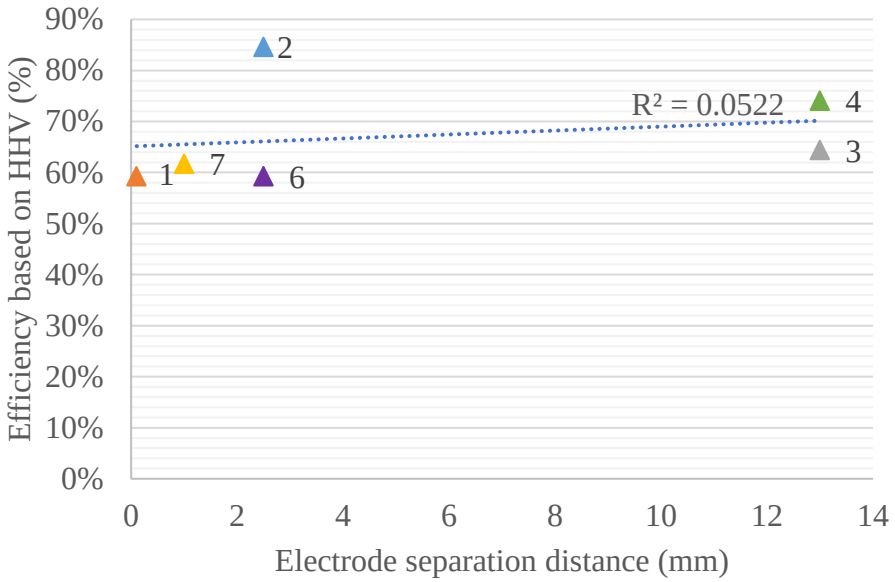

Figure 28 – Graph showing electrode separation distance and HHV efficiency at 100 mA/cm^2 for Membrane-less Devices No. 1, 2, 3, 4, 6 and 7.

Reynolds' Number Versus HHV Efficiency

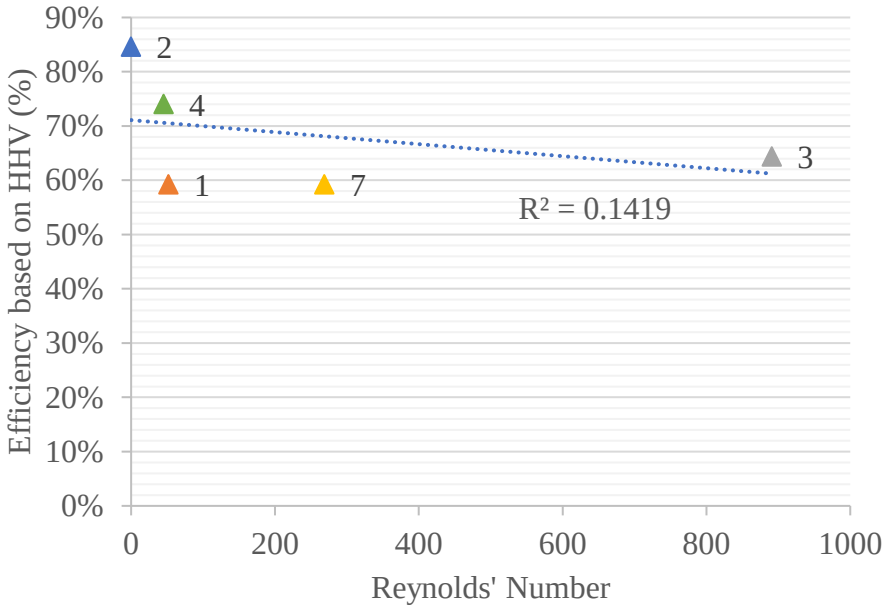

Figure 29 - Graph showing Reynolds' number of flow in Membrane-less Devices No. 1, 2, 3, 4 and 7 plotted against HHV efficiency of device at 100 mA/cm^2.